Energy Conversion and Management 271 (2022) 116308

Contents lists available at ScienceDirect

Energy Conversion and Management

journal homepage: www.elsevier.com/locate/enconman

Evolutionary based Pareto optimization algorithms for bi-objective PV array reconfiguration under partial shading conditions

Xiaoshun Zhang [a,b], Die Meng [c], Wenji Li [c,e,*], Tao Yu [d], Zhun Fan [c,e], Zhifeng Hao [c]

[a] Foshan Graduate School of Innovation, Northeastern University, 528311 Foshan, China
[b] College of Information Science and Engineering, Northeastern University, 110819 Shenyang, China
[c] College of Engineering, Shantou University, 515063 Shantou, China
[d] College of Electric Power, South China University of Technology, 510640 Guangzhou, China
[e] Key Lab of Digital Signal and Image Processing of Guangdong Province, 515063 Shantou, China

ARTICLE INFO

Keywords:
PV array reconfiguration
Bi-objective optimization
Evolutionary optimization algorithms
Partial shading condition

ABSTRACT

During the daily operation of photovoltaic array, it easily faces the partial shading conditions resulted from the cloud shadow, dropping dust, etc. It will directly cause a lifetime reduction and a generation efficiency decrement for the photovoltaic array. To weaken the negative influence of partial shading condition, one of the most favoured ways is the photovoltaic array reconfiguration. However, the conventional photovoltaic array reconfiguration only aims to maximize the power output, which did not consider the lifetime and control complexity of switching devices. To fill up this gap, this paper constructs a new bi-objective optimization of photovoltaic array reconfiguration, which attempts to simultaneously maximize the output power and minimize the switching number. Consequently, it can dramatically reduce the switching control complexity while improving the generation efficiency, while the operation life of the switching devices can be lengthened. In order to find a high-quality Pareto optimal reconfiguration schemes, six frequently-used evolutionary multi-objective optimization algorithms are employed to solve this bi-objective optimization. The effectiveness of bi-objective optimization of photovoltaic array reconfiguration is tested on three scales of total-cross-tied photovoltaic arrays under four partial shading patterns. The simulation results show that the maximum power increment by the proposed technique is up to 26.6% against to that without optimization, while the average switch number decrement is up to 31.1% compared with the single-objective optimization algorithms.

1. Introduction

Renewable energy plays an important role in the sustainable development of modern society along with reduction of fossil fuels, the expansion of population and the deterioration of the environment. Among all the renewable energy types, the solar energy has particularly attracted more and more attentions due to its abundant availability and zero carbon emission [1]. However, there are many challenges to make full use of solar energy. When the photovoltage (PV) array is shaded by surrounding buildings, dust or clouds passage [2], the modules generate different currents, but photovoltaic modules connected in series will flow through the same current. When the current flowing through the component is larger than the photoelectric current of the shaded component, the shaded component will become the load consuming branch power, thus the hot spot effect will be appeared [3]. In general, the damage of PV array can be prevented by the parallel bypass diodes. But when the bypass diodes are switched on, the PV array are short-circuited, thereby a generation power decrement is resulted for the PV array [4]. Additionally, these partial shading conditions (PSC) easily cause multi-peaks on the power-voltage (P-V) curve and chaos in maximum power point tracking (MPPT) [5].

To weaken the negative influence by PSC, various interconnection topologies have been designed for PV array, including (i) series–parallel (SP), (ii) bridged-link (BL), (iii) honey-comb (HC) and (iv) total cross tied (TCT) [6]. In [7], these topologies were studied and compared in terms of maximum power and fill factor. Among all these topologies, SP is the most practically used topology due to its simplicity [8]. However, it easily results in a power decrease by the mismatch loss under PSC [9]. To overcome this issue, the TCT topology developed from SP is promoted by connecting the connectors on each line junction, which has been proven in [10] that TCT outperformed SP, BL, and HC on the

* Corresponding author.
E-mail address: liwj@stu.edu.cn (W. Li).

https://doi.org/10.1016/j.enconman.2022.116308
Received 30 May 2022; Received in revised form 27 September 2022; Accepted 28 September 2022
Available online 20 October 2022

Nomenclature

Variables

I_{cell}	output current of the PV cell
I_{Lcell}	PV cell produced current
I_{sh}	current across parallel resistance
I_d	current through diode
I_{o1}, I_{o2}	saturation currents of the diodes
R_s	series resistances
R_{sh}	parallel resistances
V_{cell}	output voltage of the PV cell
Tc	temperature of cell
I_m	output current of the PV module
V_m	output voltage of the PV module
R_S	series resistance of the PV module
R_{SH}	shunt resistance of the PV module
I_L	light generated current of the PV module
I_{Lstc}	light generated current of the PV module under the standard test condition
G	irradiation level
I_{out}	output current of the whole PV array
I_{pq}	output current of the PV module at the pth row and the qth column
V_{out}	overall output voltage
V_{mp}	output voltage of the PV modules at the pth row
n_{row}	numbers of row in the PV array
n_{col}	numbers of column in the PV array
x_{pq}^{new}	new electrical switching states of the PV module at the pth row and qth column
x_{pq}^{0}	initial electrical switching states of the PV module at the pth row and qth column
$\boldsymbol{x}_{dis}$	matrix of discrete electricity switching states
$\boldsymbol{x}_{con}^{q}$	vector of the continuous optimization variable for the PV strings at the qth column
F_1	fitness functions for the maximum power output
F_2	fitness functions for the minimum switching number
r_{ij}	an element of the normalized decision matrix $\boldsymbol{R}$
y_{ij}	numerical outcome of the ith alternative solution for the jth attribute
w	weight vector
A_j^*	jth attribute of the positive ideal solution
A_j^-	jth attribute of the negative ideal solution
$\boldsymbol{x}_{best}$	best compromise solution
$\boldsymbol{x}_i^{PF}$	ith Pareto optimal solution

Parameters

q	charge of electron
σ_1, σ_2	ideality factors
b	Boltzmann's constant
K_{SC}	short-circuit temperature coefficient
G_0	standard irradiation
T_0	standard temperature
n_s	number of series connected PV cells

Abbreviations

KCL	Kirchhoff's current law
PV	photovoltage
PSC	partial shading conditions
P-V	power-voltage
MPPT	maximum power point tracking
SP	series–parallel
BL	bridged-link
HC	honey-comb
TCT	total cross tied
S	series
EAR	electrical array reconfiguration
CSDKP	complementary SuDoKu puzzle
DS	dominance square
CS	competence square
HCPV	high concentration photovoltaic
MCR	modified circuit reconfiguration
SDGA	standard deviation genetic algorithm
WCA	water cycle algorithm
HHO	harris-hawks optimization
MHHO	modified harris-hawks optimization
MRSE	mean root square error
SDM	single diode model
DDM	double diode model
TDM	three diode model
GWO	grey wolf optimizer
PSO	particle swarm optimization
SSA	simulated annealing approach
SCA	sine cosine algorithm
MOGWO	multi-objective grey wolf optimizer
BOA	butterfly optimization algorithm
GMP	global maximum power
AEO	artificial ecosystem-based algorithm
SDPA	socio-inspired democratic political algorithm
OMAR	optimal mileage-based PV array reconfiguration
NSGA-II	nondominated sorting genetic algorithm II
SPEA2	improving strength pareto evolutionary algorithm
TOPSIS	the technique for order preference by similarity to an ideal solution
MOCell	multi-objective cellular evolutionary algorithm
PREA	promising-region-based evolutionary many-objective algorithm
RPEA	reference points-based evolutionary algorithm
SPEAR	strength pareto evolutionary algorithm based on reference direction
LN	long and narrow
LW	long and wide
SN	short and narrow
SW	short and wide
HIL	hardware-in-the-loop

maximum power output under PSC. To further reduce the cable losses in TCT, half of its interconnections were neglected and configured as BL topology [11]. Although the HC topology easily leads to less series connected PV modules than that of SP topology, but still result in a larger number of series connected PV modules than that of BL [9,12]. The comparison results showed that the TCT topology can acquire a larger maximum power output under the same PSC [13]. Consequently, it has become the most popular reconfiguration topology to minimize the mismatch losses and maximize the power output.

Following the TCT topology, many researchers have proposed various PV array reconfiguration techniques to further increase the power output [14], which can be divided into two main categories, i.e., physical reconfiguration and electrical array reconfiguration (EAR) [15,16]. Before going on, a literature review of PV array reconfiguration techniques is here given to summarize the recent findings.

Table 1
Reported methods for PV array reconfiguration under PSC.

Author	Year	Algorithm	Objective	Topology	PV array size	Advantages
M. Horoufiany *et al.* [17]	2018	SuDoKu	Power output	TCT	4 × 4, 9 × 9	Avoid ineffective dispersion and reduce line losses
S. G. Krishna *et al.* [18,19]	2019	Improved SuDoKu	Power output	TCT	9 × 9	Reduce the line losses and disperse the shading effects
C. E. Ye *et al.* [20]	2021	Complementary SuDoKu	Power output	TCT	6 × 6	Easy implementation with simple rules
D. S. Pillai *et al.* [21]	2018	Two-phase	Power output	TCT	9 × 9	Without sensor arrangement circuitry
B. Dhanalakshmi *et al.* [22]	2018	DS	Power output	TCT	5 × 5	Reduce power losses and scalability
B. Dhanalakshmi *et al.* [5]	2018	CS	Power output	TCT	9 × 9	Easy and adaptable for PV arrays of any size
R. Venkateswari *et al.* [23]	2020	Lo Shu	Power output	TCT	9 × 9	Satisfactory performance in power enhancement, fill factor and energy savings.
Y. P. Huang *et al.* [27]	2019	MCR	Power output	TCT	2 × 2, 2 × 3	Increase the output power and efficiency of an HCPV module with high dispersion ability.
A. Srinivasan *et al.* [28]	2020	Two-step	Power output	TCT	6 × 6,9 × 9,12 × 12, 18 × 9,18 × 18, 12 × 24, 30 × 48	Superior performance for a large-scale PV array
N. A. Rajan *et al.* [30]	2017	SDGA	Power output	TCT	9 × 9	Superior convergence performance
M. Karakose *et al.* [31]	2015	A novel real-time method	Power output	TCT, SP	3 × 4	Improvement in the output power of the PV array, an efficient reconfiguration strategy, real-time applicability, easy measurable parameters, and independence from panel types
A. Mahmoud *et al.* [32]	2019	WCA	Power output	TCT	10 × 10	Reduce PS power losses, shorter execution time
S. N. Deshkar *et al.* [33]	2015	GA	Power output	TCT	9 × 9	High flexibility and easy application
D. Yousri *et al.* [34]	2020	MHHO	Power output	TCT	9 × 9, 6 × 4, 6 × 20	Fast optimization speed, high quality solution
A. S. A. Bayoumi *et al.* [35]	2021	MPA	Power output	TCT	9 × 9, 16 × 16, 25 × 25	Good convergence and robust statistical analysis
D. Yousri *et al.* [36]	2020	Multi-objective grey wolf optimizer	Power output	TCT	9 × 9	Minimize the row's current levels
A. Fathy *et al.* [37]	2020	BOA	Power output	TCT, SP-TCT, BL-TCT, BL-HC	6 × 4	Easy implementation, less controlling parameters, simple construction, real time optimization
S. Mohanty *et al.* [38]	2015	GWO	Power output	SP	2 × 2	Robust and exhibits faster convergence, fewer parameters for adjustment and less operators
D. Yousri *et al.* [39]	2020	AEO	Power output	TCT	9 × 9, 6 × 20, 16 × 16, 25 × 25	Superior performance on robustness and reliability
B. Yang *et al.* [40]	2021	Socio-inspired democratic political algorithm	Power output	TCT	10 × 10, 15 × 15, 20 × 20	Effectively reduce power losses, improve power generation efficiency and accelerate convergence rate.
X. Zhang *et al.* [41]	2021	Swarm reinforcement learning	Power output and power fluctuation	TCT	10 × 10	Reduce the optimization difficulty of OMAR, real-time generation schedule
X. Zhang *et al.* [42]	2022	An efficient multi-agent negotiation algorithm	Total profit with hydrogen selling profit and regulation cost	TCT	10 × 10	Increase the total profit, achieve an efficient and distributed optimization

1.1. Literature review of PV array reconfiguration techniques

The physical reconfiguration only changes the physical position of PV modules instead of the electrical connections, thus it is simpler and cheaper as it does not require a complex and dynamic operation for multiple switching devices. According to this manner, a SuDoKu puzzle method [17] was proposed to configure the PV modules in the array so as to enhance the generated power. This structure facilitates to distribute the effect of shading over the array, thereby reducing the occurrence of shading of modules in the same row. However, the line losses that depend on the length of the wire requirement of connection is not considered. In [18,19], an improved SuDoKu was designed to solve the limitation of the original SuDoKu puzzle technique. In [20], a complementary SuDoKu puzzle (CSDKP) technique for the circuit reconfiguration of PV arrays and an especially designed complementary diagonal circuit arrangement were proposed. The simulation results [20] demonstrated that CSDKP reduced the averaged power loss of 12.86 % and enhanced the averaged maximum-power improvement of 14.6 % under PSC. A new two-phase method [21] was tested for dispersing the shadow of any size in two different phases, which was useful in relocating PV panels to enhance the power output. As a result, the two-phased technology can realize an average of 6 % power improvement against to TCT [21] for a 9 × 9 PV array. In [22], the dominance square (DS) was designed to further reduce the mismatch loss. Compared with DS, the competence square (CS) [5] is simpler for application and can achieve maximum power enhancement of up to 8.7 %. Different from SuDoKu, DS, and CS, the Lo Shu technique [23] can achieve a more efficient shadow dispersion through fewer shifts of panels. Based on the screw pattern in the row formation, a static array configuration method [24] was proposed to improve the power output, which can perform better than TCT and SuDoKu puzzle technique. In [25], a novel knight pattern array configuration scheme was designed based on the movement of the chess coin, which can effectively enhance the power conversion efficiency.

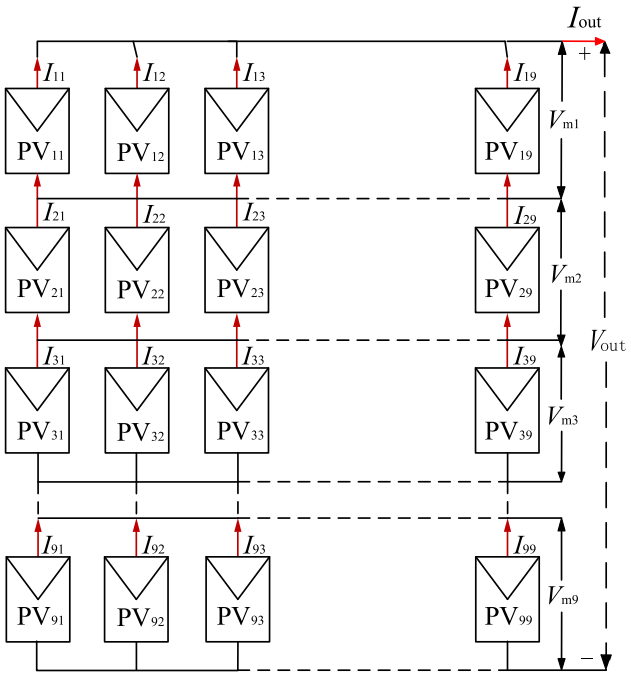

Fig. 1. A 9 × 9 TCT connected PV array.

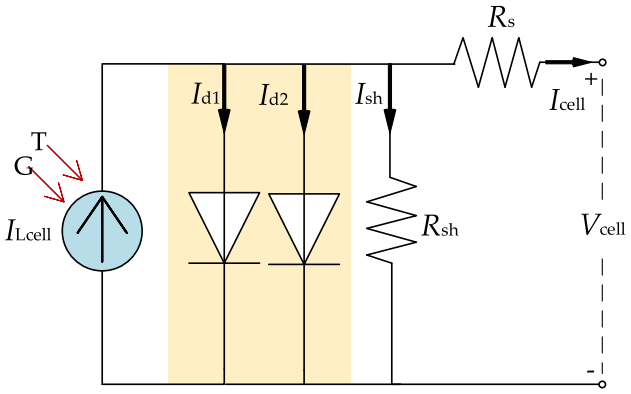

Fig. 2. Equivalent circuits of PV cell.

Table 2
Execution procedure of evolutionary based Pareto optimization algorithm for bi-objective PV array reconfiguration.

1: Initialize the parameters and the population;
2: Input the real-time irradiation distribution and temperature for the PV array;
3: Set $k = 1$;
3: **While** $k \leq k_{max}$
4: Calculate the fitness functions of each individual by Eq. (11);
5: Determine the Pareto dominance relationships between different individuals;
6: Update the Pareto solution repository with the new non-dominated solutions;
7: Implement the exploration and exploitation based on the current Pareto solution repository;
8: **End While**
9: Output the Pareto optimal solutions and Pareto front for bi-objective PV array optimization.

Compared with the physical reconfiguration, EAR is a technique of dispersing shadows on the PV array by rearranging the shaded PV panels via changing the electrical connection states instead of the physical location [26]. As a result, the shadows on the PV array are more evenly distributed in real time. In [27], a modified circuit reconfiguration (MCR) technique was proposed for high concentration photovoltaic

Table 3
The main parameter of PV module.

Parameters	Value
Module	A10 Green Technology A10J-M60-225
Number of parallel strings	1
Number of series-connected modules per string	1
Number of cells per module (N_{cell})	60
Maximum power per module (W)	224.9856
Open circuit voltage per module (V)	36.24
Short-circuit current per module (A)	8.04
Voltage at the maximum power point per module (V)	30.24
Current at the maximum power point per module (A)	7.44

Table 4
The main parameters used in different algorithms.

Algorithm	Parameter	Value
NSGA-II	Crossover probability	1
	Mutation probability	1(or 0.5)
	Variation index	20
	Max fitness evaluation	10,000
SPEA2	Mutation probability	1
	Variation index	20
	Probability of crossover	1
MOCell	Probability of mutation and crossover	1
	Distribution index of mutation and crossover	20
PREA	Probability of partner selection	0.7
	Ratio of individuals being used to generate reference points	0.4
	Distribution index of mutation and crossover	20
RPEA	Ratio of individuals being used to generate reference points	0.4
	Parameter determining the difference between the reference point and the individuals	0.1
SPEAR	Mutation probability	1
	Variation index	20

modules under PSC. The reliability tests in [27] demonstrated that the daily energy harvested from the rectangular module was improved around 15 %. A hybrid reconfiguration algorithm [28] has been proposed to suppress the harmful effect by PSC, which can also reduce the required numbers of switches and the dimension of the switching matrix circuit. In essence, electrical array reconfiguration (EAR) is a mixed integer quadratic programming, in which the optimization complexity will increase exponentially as the PV array scale increases [29,26]. Therefore, many *meta*-heuristic algorithms were introduced to solve this problem due to their excellent application flexibility and global searching ability. In order to search an optimal switching matrix, a standard deviation genetic algorithm (SDGA) [30] was presented to determine the final connection matrix for the new electrical interconnection, which can minimize the standard deviation to equalize the individual row currents. A novel real-time method that based on an artificial neural network [31] was developed an optimal reconfiguration for a 3 × 4 PV array. As shown in results, the novel real-time method made contributions on real-time applicability and easy measurable parameters. In [32], a water cycle algorithm (WCA) was applied in PV array reconfiguration to reduce the power losses and the irradiance level mismatch index. The simulation results in [32] demonstrated that the power enhancement by WCA was up to 37.88 % compared with TCT, while the execution time of WCA was faster than that of TCT for the same problem. In order to mitigate the shading effects, the harris-hawks optimization (HHO) [33] and the modified harris-hawks optimization (MHHO) algorithm [34] were used for PV reconfiguration on the 9 × 9 and 6 × 20 TCT connected arrays, which can acquire more power compared with TCT, competence square (CS), particle swarm

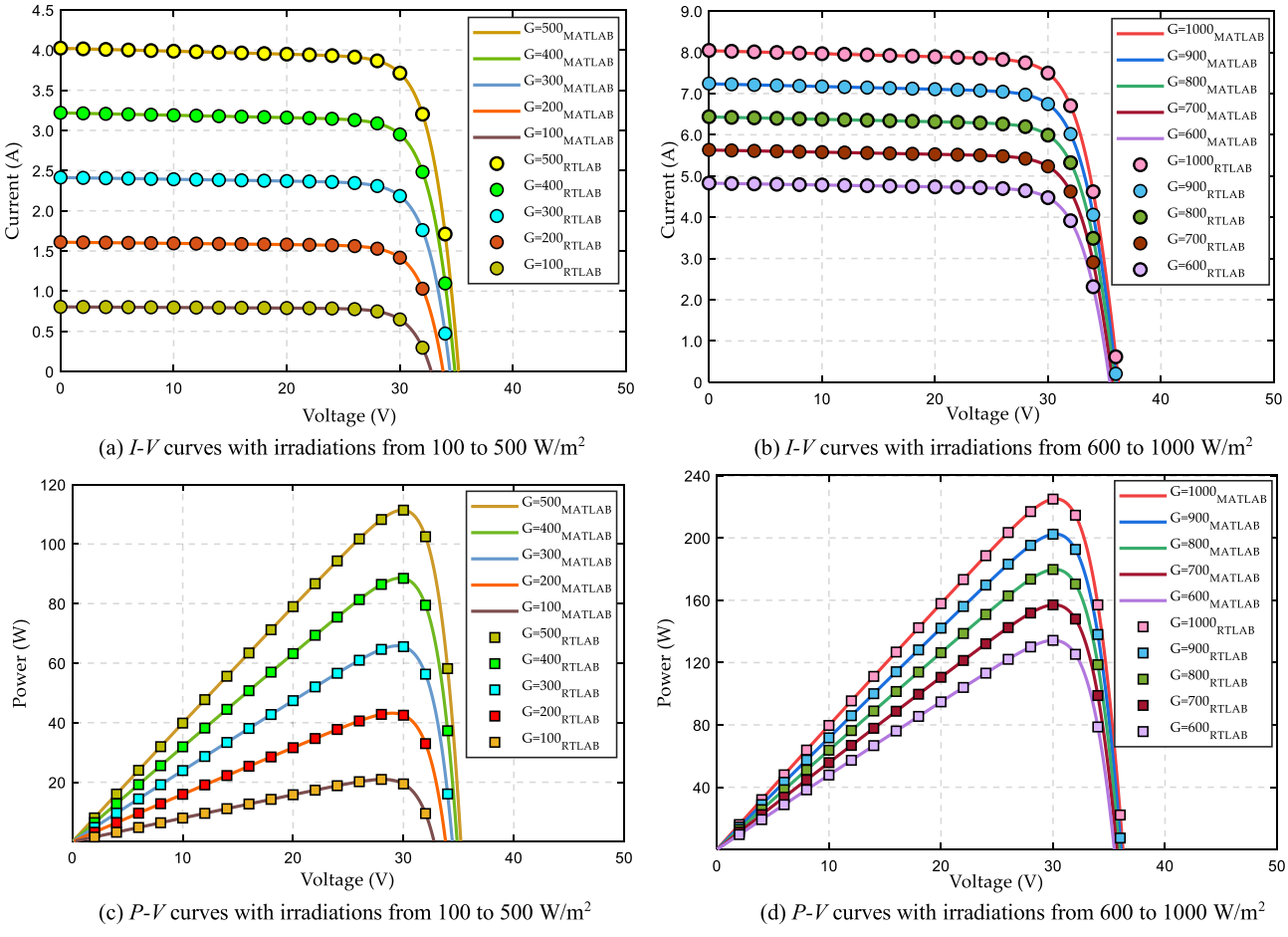

(a) *I-V* curves with irradiations from 100 to 500 W/m^2

(b) *I-V* curves with irradiations from 600 to 1000 W/m^2

(c) *P-V* curves with irradiations from 100 to 500 W/m^2

(d) *P-V* curves with irradiations from 600 to 1000 W/m^2

Fig. 3. Output curves of each PV module obtained by RTLAB and MATLAB platforms under various irradiations with $T_c = 25$℃.

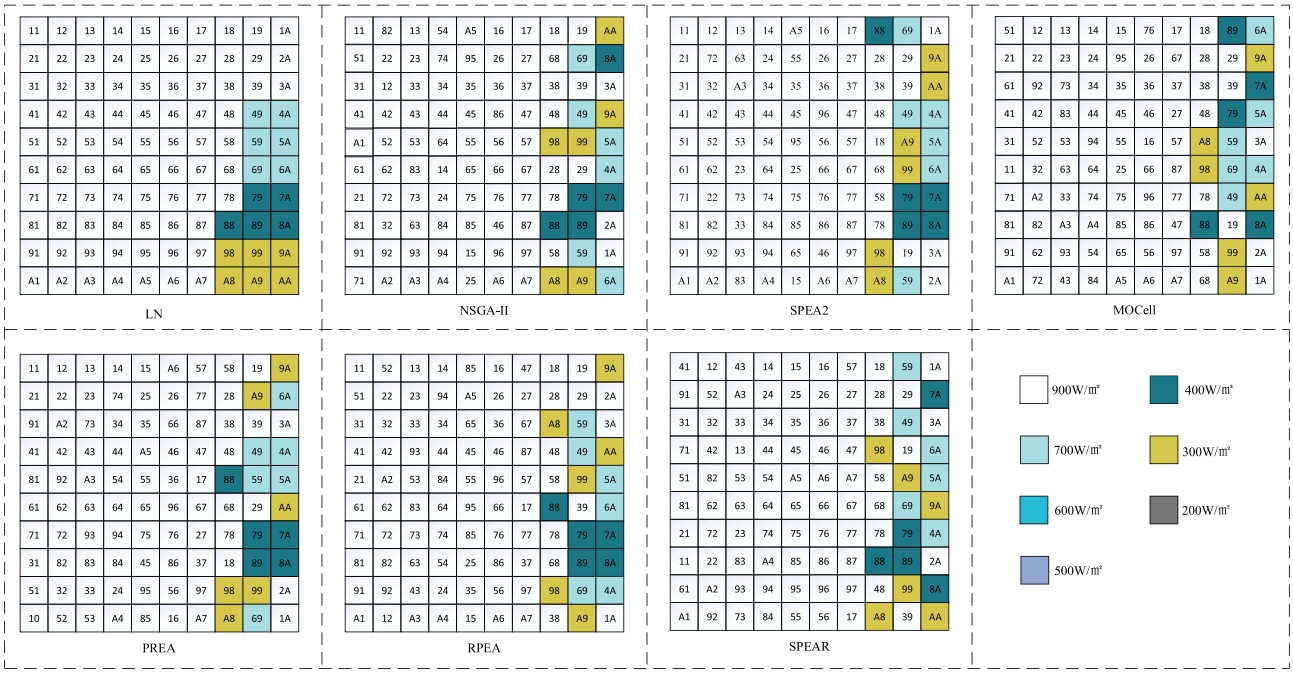

Fig. 4. The optimal PV reconfiguration schemes obtained by different algorithms on a 10 × 10 PV array under LN case.

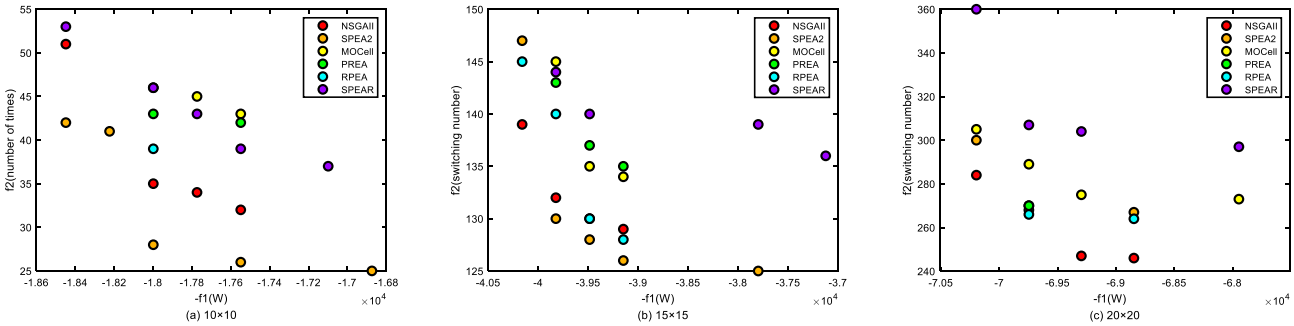

Fig. 5. The Pareto fronts derived by different algorithms for different PV arrays under LN case.

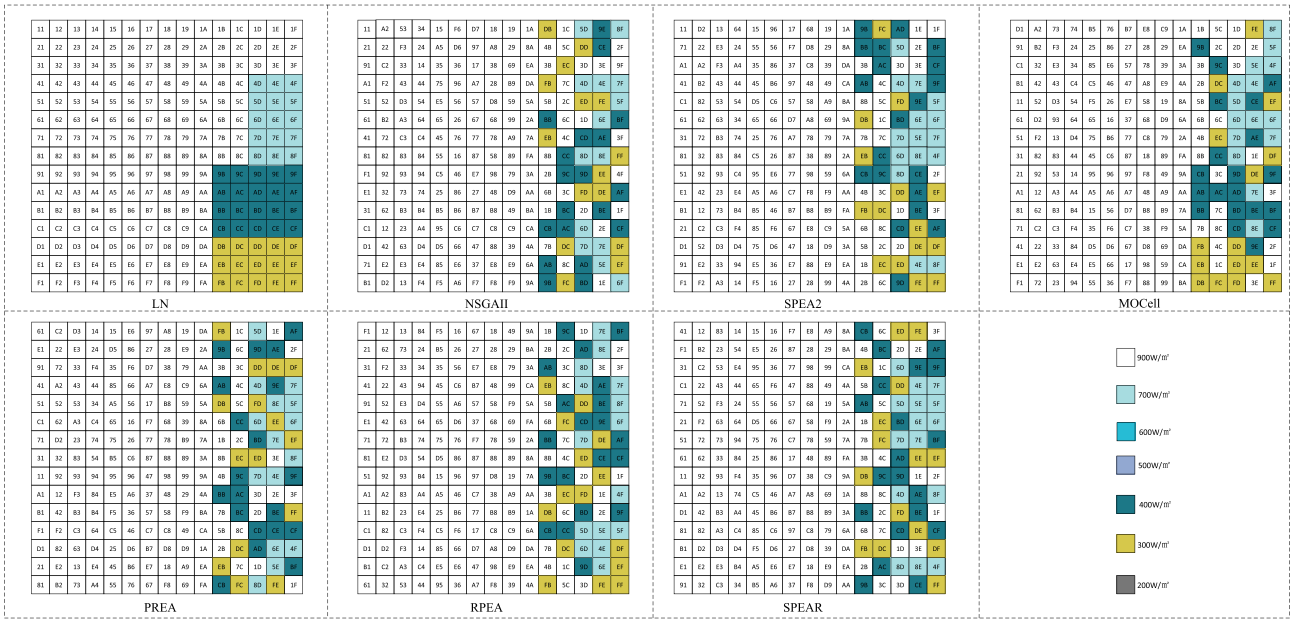

Fig. 6. The optimal PV reconfiguration schemes obtain by different algorithms on a 15 × 15 PV array under LN case.

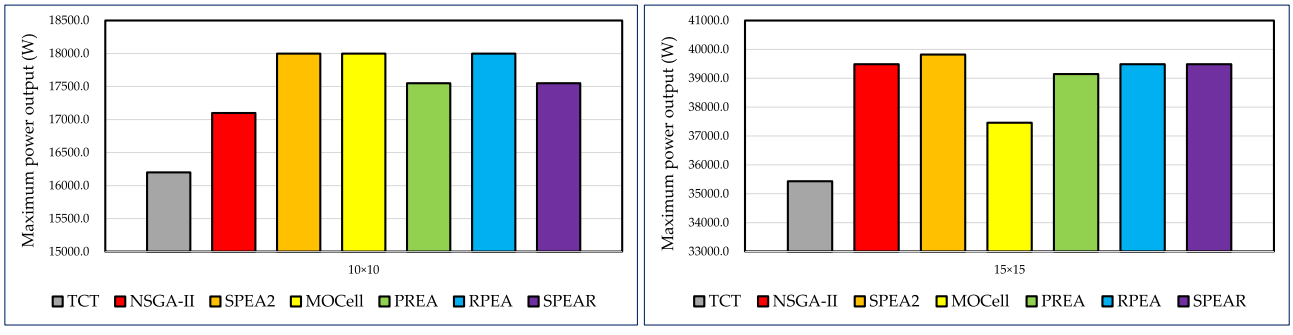

(a) 10×10 PV array (b) 15×15 PV array

Fig. 7. Theoretical maximum power outputs obtained by different algorithms under LN case.

optimization (PSO). A new objective function named the mean root square error (MRSE) was considered in the marine predators algorithm (MPA) [35], which has been proven with higher robustness and larger power increasement compared with grey wolf optimization (GWO), simulated annealing approach (SAA), PSO, and sine cosine algorithm (SCA). In [36], a multi-objective grey wolf optimizer (MOGWO) was applicable for PV array reconfiguration to minimize the difference between the adjacent row current. The results comparisons in [36] divulged that MOGWO enhanced the percentage of power in a range of 9.4 % to 18.8 % against to TCT and 1.4 % to 8.6 % against to the modified SuDoKu. In [37], a new bio-inspired algorithm called butterfly optimization algorithm (BOA) was designed to extract more output power of PV system under PSC against to the GWO [38] under some shadow patterns. The proposed BOA succeeded in achieving a power output increasement of 27.43 % compared with SP-TCT configuration. The artificial ecosystem-based algorithm (AEO) [39] with an innovation fitness function was adopted in PV array reconfiguration, which revealed the innovative fitness function can tackle the issue of the

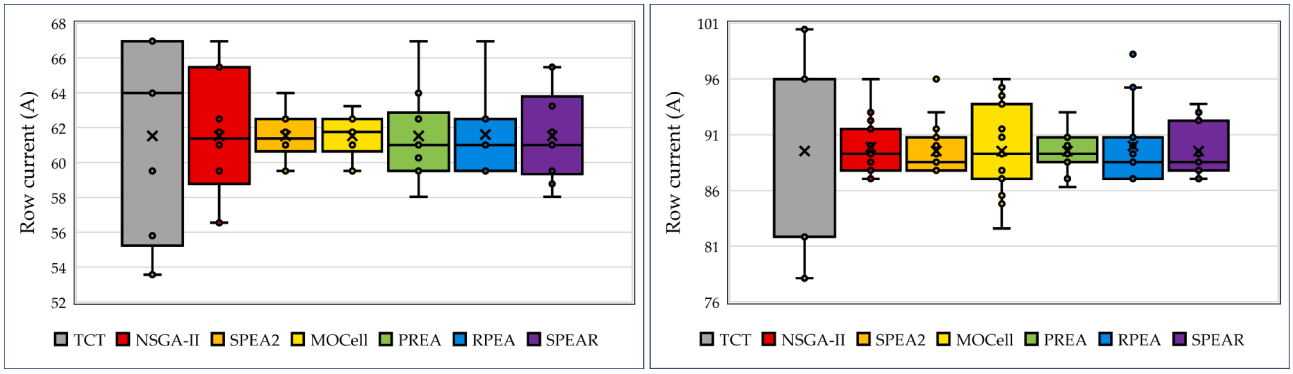

(a) 10×10 PV array (b) 15×15 PV array

Fig. 8. Boxplot of row currents obtained by different algorithms under LN case.

weight coefficient can significantly affect the quality of solution. In [40], a socio-inspired democratic political algorithm (SDPA) was proposed to mitigate the effect of partial shading on the power output and circuit. Simulation results demonstrate that SDPA can enhance output power of photovoltaic array by 21.47 %,21.55 % and 20.98 % for a 10 × 10 (small) PV array, a 15 × 15 (medium) PV array and a 20 × 20 (large) PV array respectively compared to TCT interconnection scheme. Except the maximum power output increasement under PSC, a new optimal mileage-based PV array reconfiguration [41] was designed by further taken the power fluctuation into account. In addition, a new multi-period PV array reconfiguration with a hydrogen energy storage system [42] was constructed to maximize the total profit of a PV system instead of maximizing the power output, in which the additional hydrogen selling profit and the regulation cost caused by the power fluctuation were considered in the total profit. In [43], a new dynamic reconfiguration technique with a switching controller was formulated, which was tested on a 6 × 6 TCT connected PV array by varying the switching matrix between the fixed part and adaptive part. The simulation results [43] showed that the proposed method significantly reduced the number of connected switches by 35 % compared to the other dynamic reconfiguration methods.

1.2. Research gaps and the novelty of this work

In summary, the existing studies of PV array reconfigurations only consider the maximum the power output via a single-objective optimization, as shown in Table 1. Except the power output, the additional hydrogen selling profit and regulation cost resulted from the power fluctuation were considered [41,42]. However, the existing works did not consider the lifetime and control complexity of switching devices during the PV array reconfiguration. Additionally, the single-objective optimization can only provide a single optimal reconfigurable scheme for the PV array. Consequently, it will easily shorten the lifetime of switching devices and increase the control complexity of PV array reconfiguration. Besides, it will result in a low flexibility of operation choice for PV array reconfiguration with a single scheme. Hence, this paper constructs a new bi-objective PV array reconfiguration to resolve these problems, which attempts to maximize the power output and minimize switching number of electrical connections simultaneously. Compared with the traditional PV array reconfiguration, the presented bi-objective PV array reconfiguration is a more complex Pareto optimization with two competing and conflicting objective functions. To find a high-quality Pareto front, the evolutionary based Pareto optimization algorithms such as nondominated sorting genetic algorithm II (NSGA-II) and the improving strength pareto evolutionary algorithm (SPEA2), are suitable and competent to address this problem because of their model-free feature and strong global searching ability. Consequently, this work adopts the evolutionary based Pareto optimization algorithms to solve the bi-objective PV array reconfiguration, which contains the following novelties:

- Based on the conventional EAR, a bi-objective PV array reconfiguration is firstly constructed by considering the switching control complexity except the maximum power output, which can effectively achieve a Pareto tradeoff between these two objective functions, thus the high operation economy can be guaranteed.
- Various evolutionary based Pareto optimization algorithms are designed for the bi-objective PV array reconfiguration, which can acquire multiple high-quality Pareto optimal reconfiguration schemes for the PV array. Hence, the operation flexibility of PV array can be significantly improved as it can select a proper reconfiguration scheme according to dynamic preference on maximum power output or the switching control complexity. Moreover, an ideal point based decision making method is employed to determine the best compromise reconfiguration scheme due to its simple fast calculation and proper balance between two objective functions.

The rest of this work is organized as follows: Section 2 gives the mathematical model of bi-objective PV array reconfiguration; Section 3 provides the design process of evolutionary based Pareto optimization algorithms for bi-objective PV array reconfiguration and the technique for order preference by similarity to an ideal solution (TOPSIS). In Section 4, the case studies are given and discussed. At last, Section 5 presents the conclusion.

2. System description

2.1. Modelling of PV array

A PV array consists of numerous series–parallel PV modules, in which PV module is composed of numerous series–parallel PV cells [44], as shown in Fig. 1. It is essential to analyze the electrical characteristic of PV cell for the application of the reconfiguration technique [45]. In general, the PV cell can be described with a single-diode or multi-diode models [46]. To balance the modelling simplicity and accuracy, the double-diode model is introduced in this work, as shown in Fig. 2.

According to Kirchhoff's current law (KCL), the total current generated by a double-diode PV cell can be calculated as follows:

$$I_{cell} = I_{Lcell} - I_{d1} - I_{d2} - I_{sh}\# \quad (1)$$

where I_{Lcell} is the PV cell produced current; I_{sh} is the current across parallel resistance; I_{d1} and I_{d2} are the currents through two diodes, respectively; and I_{cell} is the output current of the PV cell.

Substituting I_{sh}, I_{d1} and I_{d2} in Eq. (1), then the current equation can be given as follows:

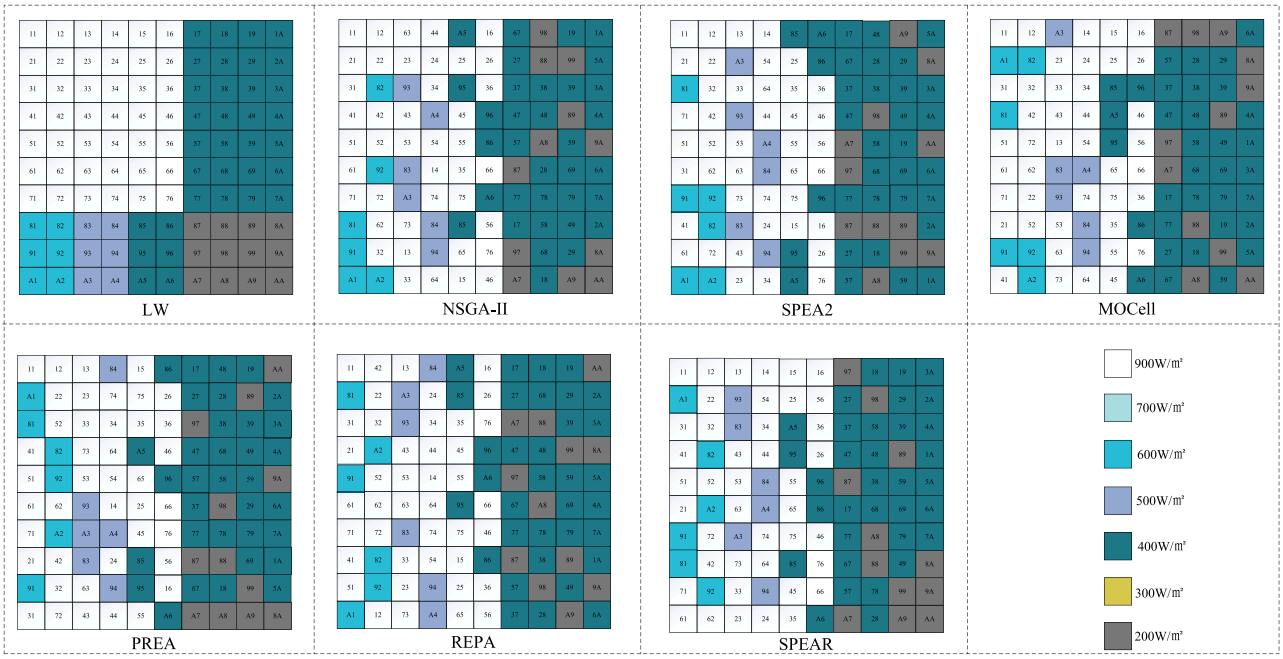

(a) 10×10 PV array

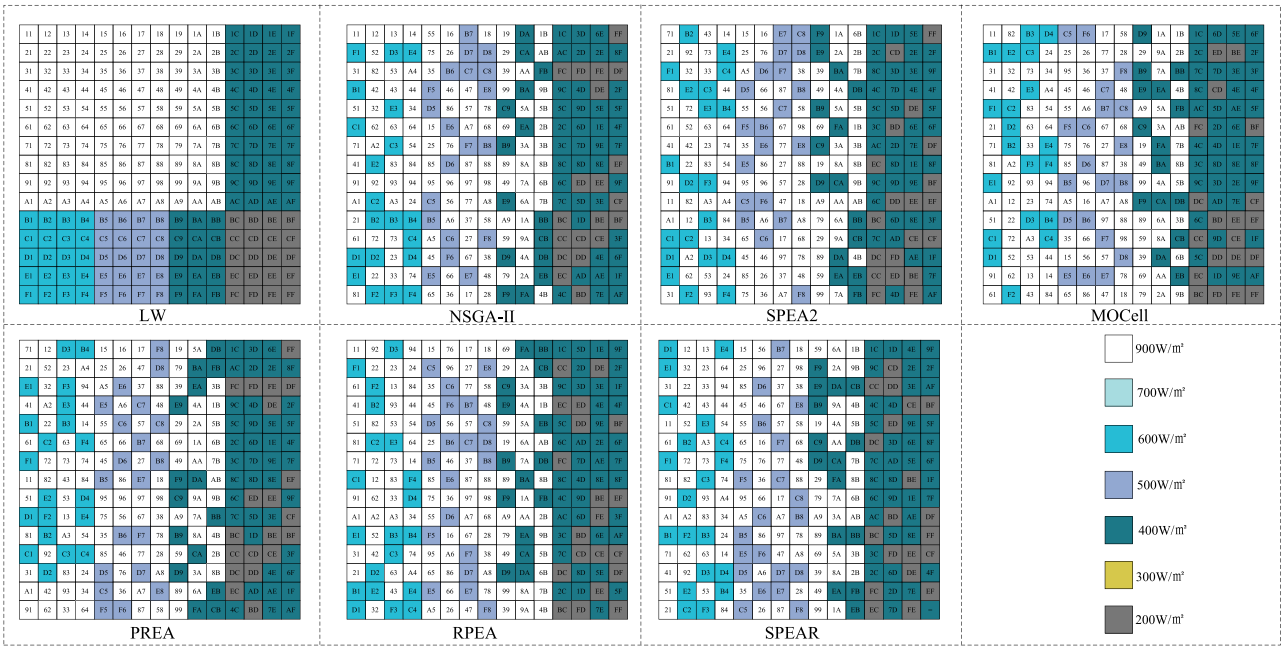

(b) 15×15 PV array

Fig. 9. The optimal PV reconfiguration schemes obtained by different algorithms on 10 × 10 and 15 × 15 PV array under LW case.

$$I_{\text{cell}} = I_{\text{Lcell}} - I_{\text{o1}}\left[exp\left(q\frac{V_{\text{cell}} + I_{\text{cell}}R_{\text{s}}}{b\sigma_1 T_{\text{c}}} - 1\right)\right] - I_{\text{o2}}\left[exp\left(q\frac{V_{\text{cell}} + I_{\text{cell}}R_{\text{s}}}{b\sigma_2 T_{\text{c}}} - 1\right)\right] - \frac{V_{\text{cell}} + I_{\text{cell}}R_{\text{s}}}{R_{\text{sh}}}\# \tag{2}$$

where I_{o1} and I_{o2} are the saturation current of the diodes; q is the charge of electron; R_{s} and R_{sh} are the series and parallel resistances, respectively; V_{cell} is output voltage of the PV cell; Tc is the temperature of cell; σ_1 and σ_2 are the ideality factors; and b is the Boltzmann's constant.

As a PV module which is connected by n_{s} series PV cells, the output current can be shown as follows:

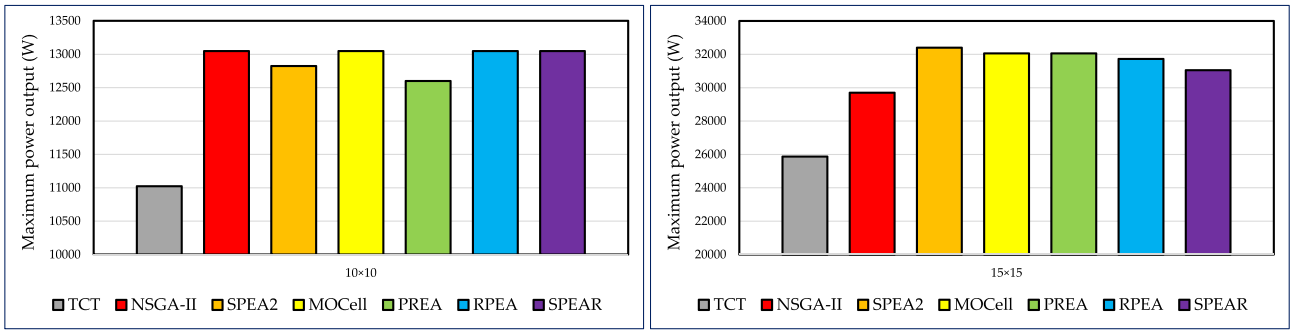

(a) 10×10 PV array (b) 15×15 PV array

Fig. 10. Theoretical maximum power outputs obtained by different algorithms under LW case.

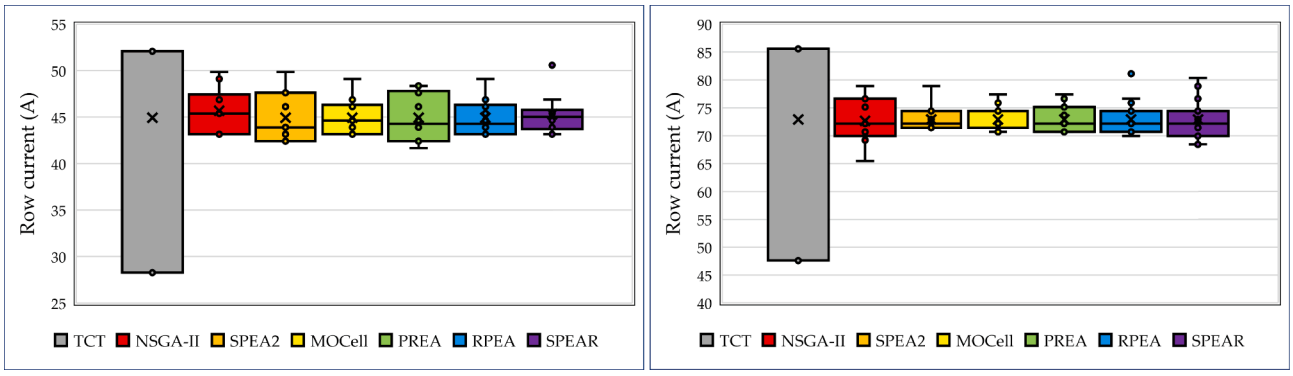

(a) 10×10 PV array (b) 15×15 PV array

Fig. 11. Boxplot of row currents obtained by different algorithms under LW case.

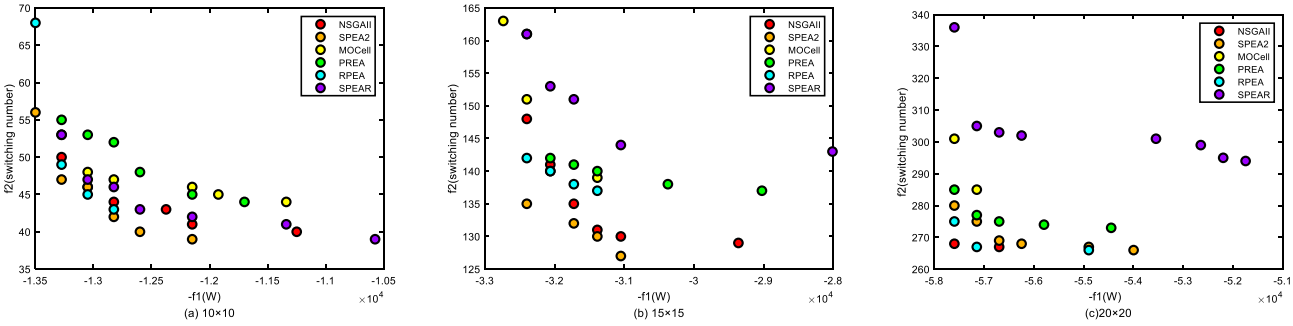

Fig. 12. The Pareto fronts derived by different algorithms for different PV arrays under LW case.

$$I_m = I_L - I_{o1}\left[exp\left(q\frac{V_m + I_m R_S}{n_S b \sigma_1 T_c} - 1\right)\right] - I_{o2}\left[exp\left(q\frac{V_m + I_m R_S}{n_S b \sigma_2 T_c} - 1\right)\right] - \frac{V_m + I_m R_S}{R_{SH}}\# \tag{3}$$

where I_m is the output current of the PV module; q is the electron charge; V_m is the output voltage of the PV module; R_S and R_{SH} are the series and shunt resistance of the PV module, respectively; and I_L is the light generated current of the PV module, which is directly influenced by the irradiation and temperature, as.

$$I_L = \frac{G}{G_0}[I_{Lstc} + K_{SC}(T_c - T_0)]\# \tag{4}$$

where I_{Lstc} is the light generated current of the PV module under the standard test condition; K_{SC} is the short-circuit temperature coefficient; G is the irradiation level (W/m^2); G_0 and T_0 are the standard irradiation and temperature (25 ℃ and 1000 W/m^2), respectively.

In the TCT configuration, the PV modules are linked in parallel by

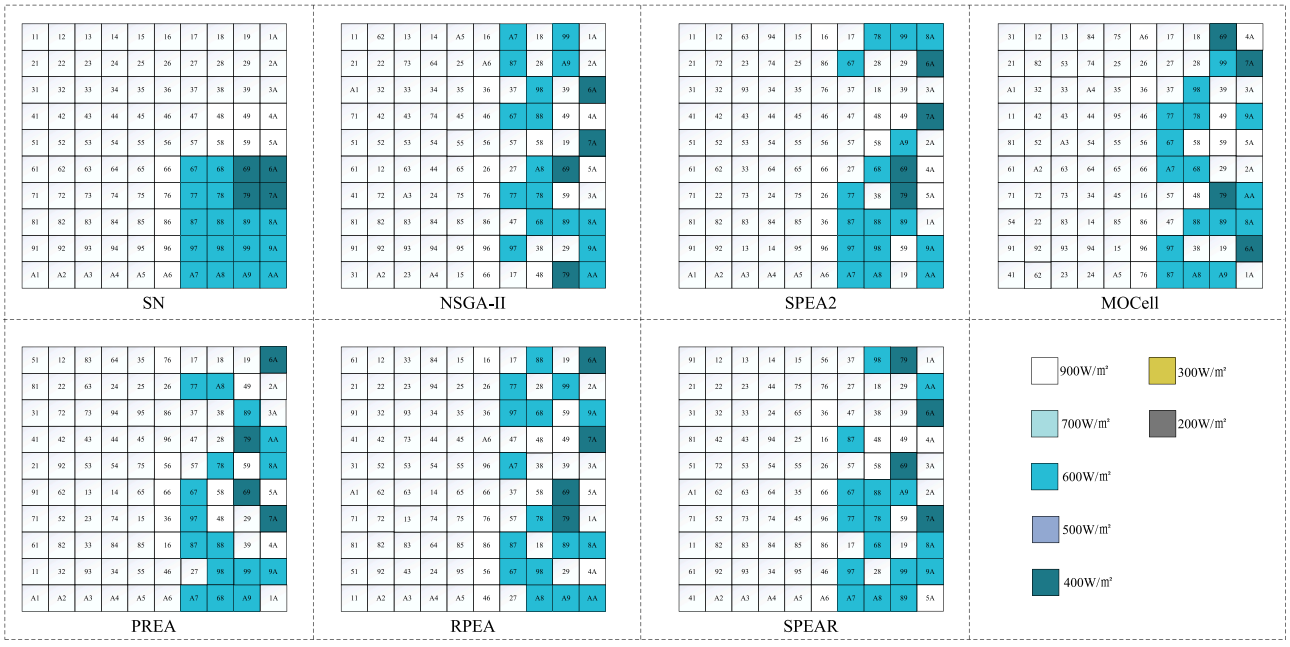

(a) 10×10 PV array

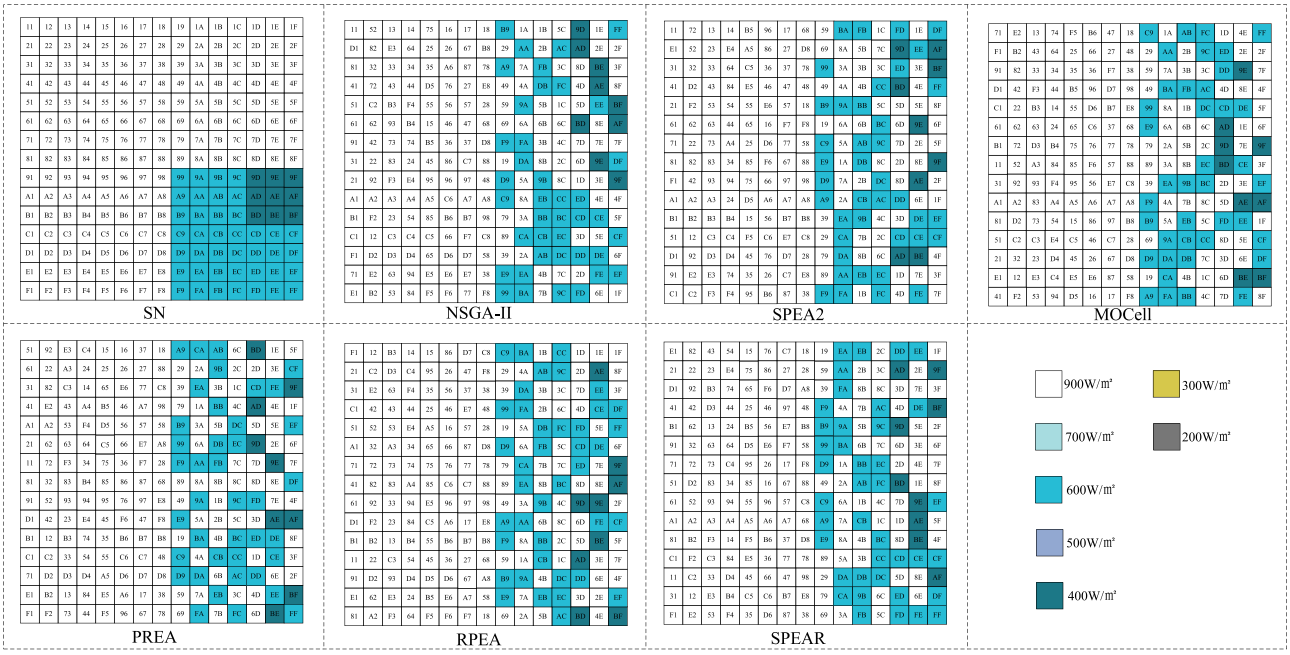

(b) 15×15 PV array

Fig. 13. The optimal PV reconfiguration schemes obtained by different algorithms on 10 × 10 and 15 × 15 PV array under SN case.

cross ties to each row, and these modules are linked in series in each column, such as a 9 × 9 TCT connected PV array in Fig. 1. Note that the TCT configuration can relocate the electrical positions in each column by interchanging a switch matrix of PV array. By applying Kirchhoff's current law and Kirchhoff's voltage law, the output current and voltage of the PV array can be calculated as.

$$I_{\text{out}} = \sum_{q=1}^{n_{\text{col}}} \left(I_{pq} - I_{(p+1)q} \right) = 0, p = 1, 2, \cdots, n_{\text{row}} \# \tag{5}$$

$$V_{\text{out}} = \sum_{p=1}^{n_{\text{row}}} V_{mp} \# \tag{6}$$

where I_{out} denotes the output current of the whole PV array; I_{pq} denotes the output current of the PV module at the pth row and the qth column; V_{out} is the overall output voltage; V_{mp} is the output voltage of the PV modules at the pth row; n_{row} and n_{col} represent the numbers of row and column in the PV array, respectively.

TCT configuration compared with other configurations, such as the SP and BL configurations, has efficient ability to advance the generated energy under partial shading. Thus, TCT reconfiguration is a preferred application among researchers. However, TCT reconfiguration has many disadvantages, such as its inability to uniformly disperse the shading through the array. in addition, TCT reconfiguration requires a number of sensors to assess the voltage, current, and radiation level for each PV panel, as presented in [47].

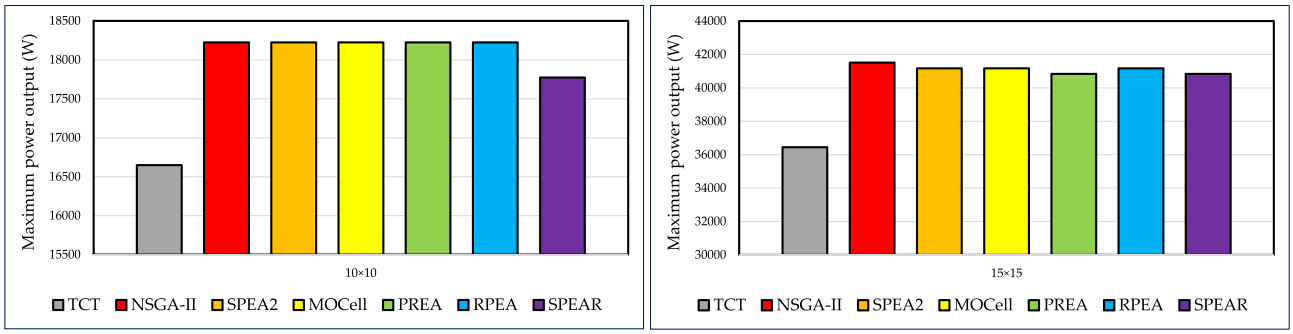

(a) 10×10 PV array (b) 15×15 PV array

Fig. 14. Theoretical maximum power outputs obtained by different algorithms under SN case.

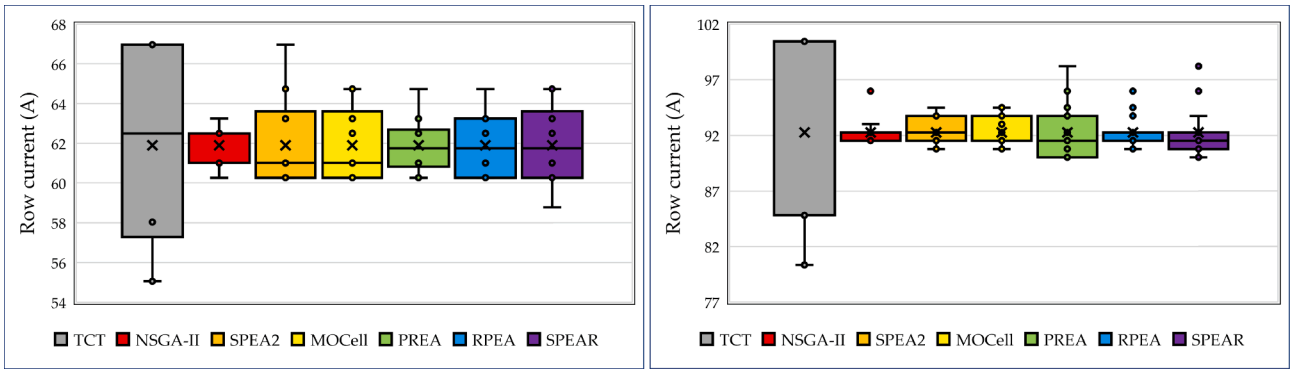

(a) 10×10 PV array (b) 15×15 PV array

Fig. 15. Boxplot of row currents obtained by different algorithms under SN case.

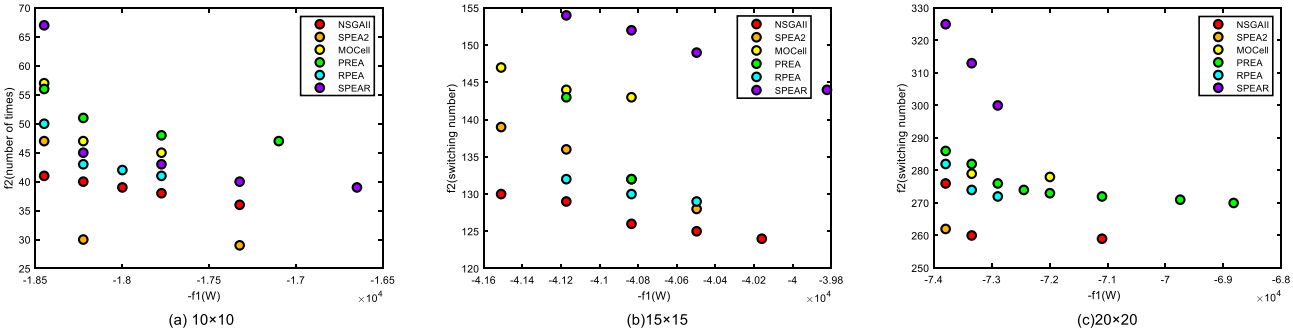

Fig. 16. The Pareto fronts derived by different algorithms for different PV arrays under SN case.

2.2. Optimization model of PV array reconfiguration

In this work, the bi-objective PV array reconfiguration contains two objective functions, including the maximum power output and the minimum switching number of electrical connections. These two objective functions can be sought while satisfying the switching constraint, i.e., each PV module can only exchange its electrical switching state with another PV module in the same column. As a result, the bi-objective optimization of PV array reconfiguration can be described as follows:

$$\begin{cases} \max f_1 = V_{\text{out}} \times I_{\text{out}} \\ \min f_2 = \sum_{p=1}^{n_{\text{row}}} \sum_{q=1}^{n_{\text{col}}} sign\left(\left|x_{pq}^{\text{new}} - x_{pq}^{0}\right|\right) \end{cases} \# \tag{7}$$

The reconfiguration of PV array also needs to consider the constraints of electrical switches, as follows:

$$s.t. \begin{cases} x_{pq}^{\text{new}} \in \{1, 2, \cdots, n_{\text{row}}\}, p = 1, 2, \cdots, n_{\text{row}}; q = 1, 2, \cdots, n_{\text{col}} \\ \bigcup_{p=1}^{n_{\text{row}}} x_{pq}^{\text{new}} = \{1, 2, \cdots, n_{\text{row}}\}, q = 1, 2, \cdots, n_{\text{col}} \end{cases} \# \tag{8}$$

where *sign* denotes the sign function with $sign(x) = 0$ If $x = 0$ and $sign(x) = 1$ If $x > 0$; x_{pq}^{new} and x_{pq}^{0} represent the new and initial electrical switching states of the PV module at the pth row and qth column, respectively.

3. Proposed PV array reconfiguration technique

In this work, six frequently-used evolutionary based Pareto optimization algorithms including NSGA-II, SPEA2, multi-objective cellular

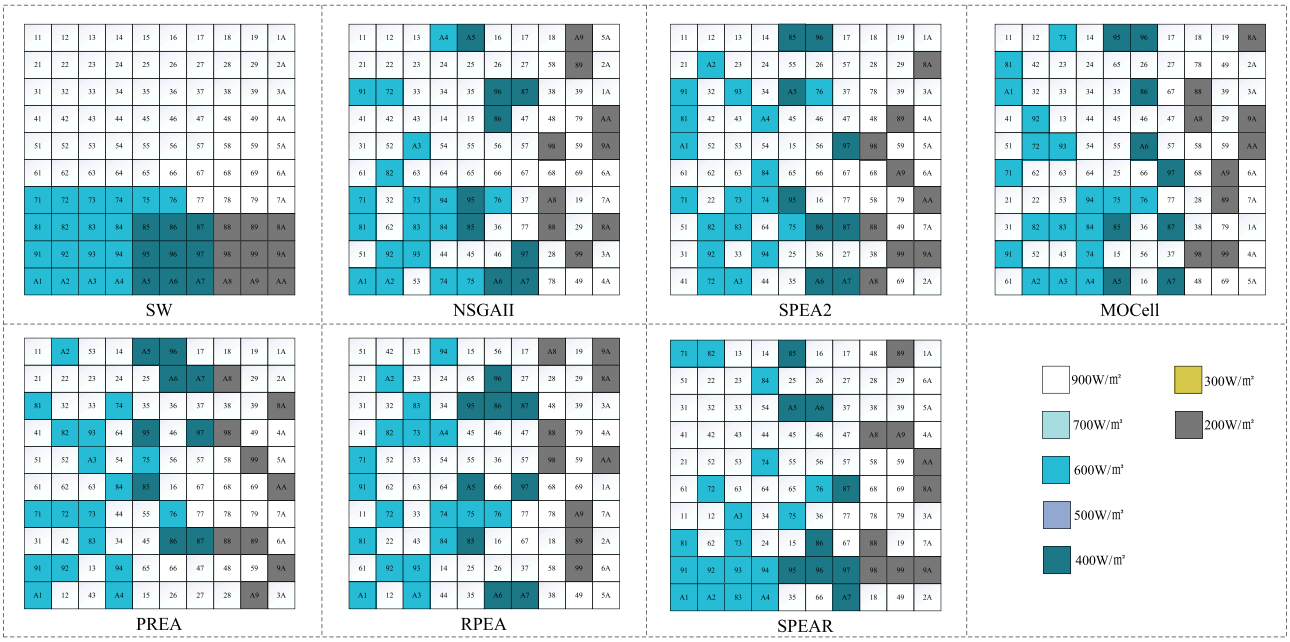

(a) 10×10 PV array

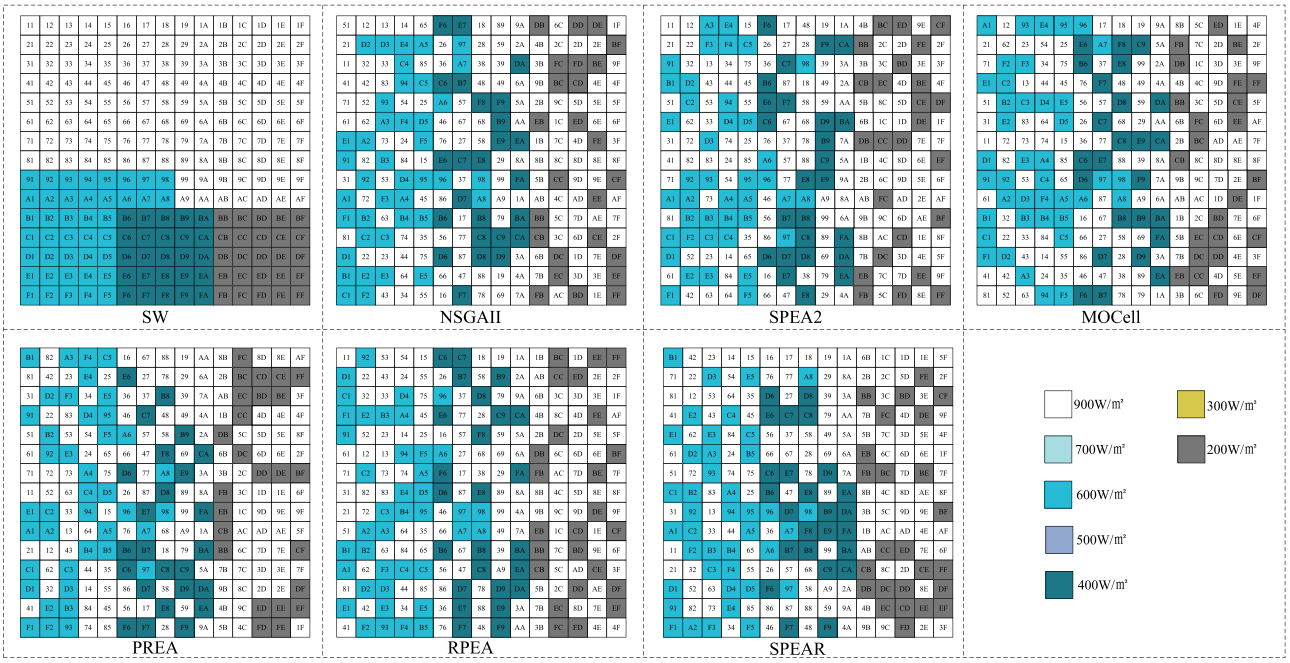

(b) 15×15 PV array

Fig. 17. The optimal PV reconfiguration schemes obtained by different algorithms on 10 × 10 and 15 × 15 PV array under SW case.

evolutionary algorithm (MOCell), a promising-region-based evolutionary many-objective algorithm (PREA), a reference points-based evolutionary algorithm (RPEA), and a strength pareto evolutionary algorithm based on reference direction (SPEAR) are introduced for bi-objective PV array reconfiguration. Note that there are no innovations of the optimization principles for these optimization algorithms in this work. According to the Pareto optimal solutions obtained by these algorithms, the TOPSIS [48] is employed to determine the best compromise PV reconfiguration scheme.

3.1. Methodology

Here, the operators of the presented evolutionary based Pareto optimization algorithms are in line with their original optimization principles [49]-[54], as follows:

(i) **NSGA-II:** it uses an elitism based non-dominated sorting method for ranking and sorting each individual and a crowding distance approach in its section operator for keeping the diversity among the obtained Pareto optimal solutions [49]. In the non-dominated sorting, the objective functions are firstly evaluated for each solution, and then the whole population is sorted into different

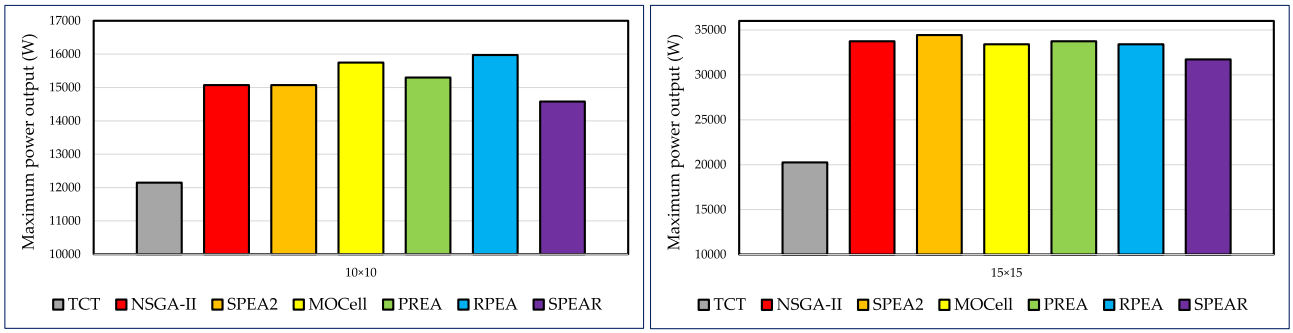

(a) 10×10 PV array (b) 15×15 PV array

Fig. 18. Theoretical maximum power outputs obtained by different algorithms under SW case.

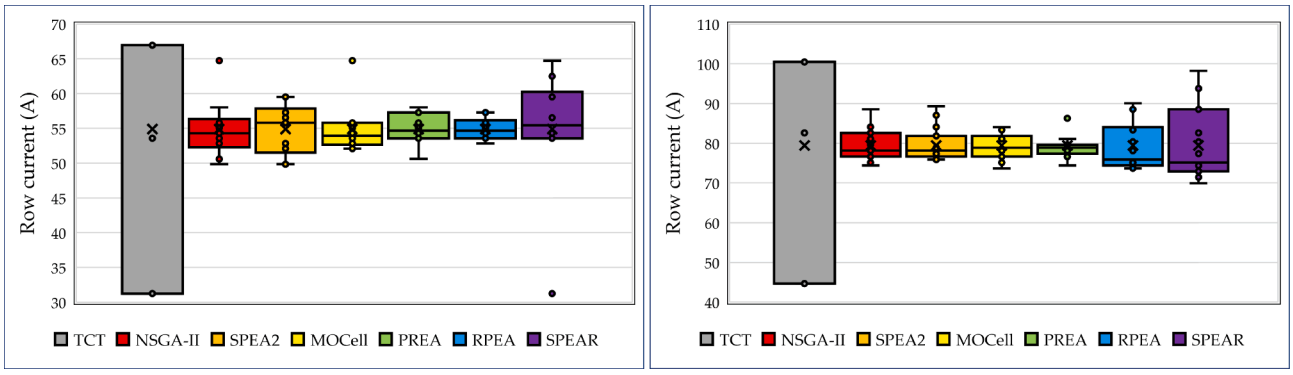

(a) 10×10 PV array (b) 15×15 PV array

Fig. 19. Boxplot of row currents obtained by different algorithms under SW case.

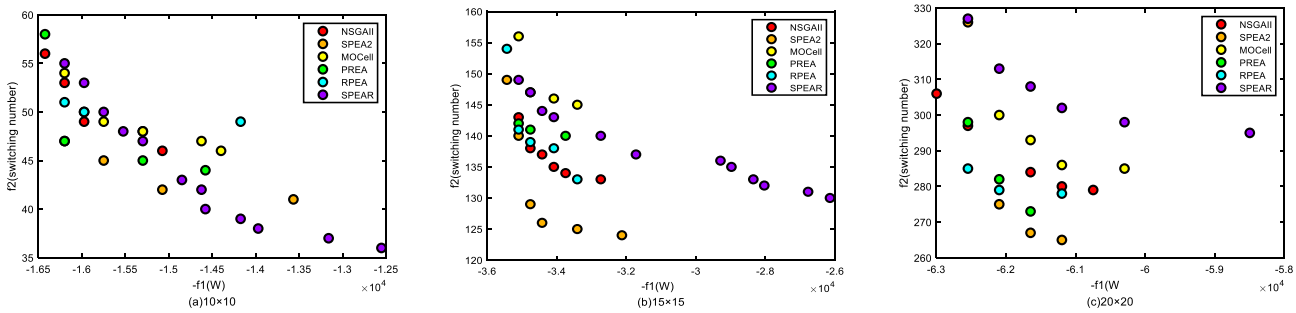

Fig. 20. The Pareto fronts derived by different algorithms for different PV arrays under SW case.

nondomination levels based on the calculated dominance count and ranks. Secondly, the population is sorted in ascending order, thus the smallest and the largest function values for each objective are selected as boundary values and an infinite crowding distance value is assigned to them. The crowding distance between any two neighboring solutions is then calculated based on the normalized difference in the objective function value.

(ii) **SPEA2**: it uses an external archive which includes the previously found non-dominated solutions, which is updated after every generation and for each solution a strength value is computed [50]. Based on this computed strength values the fitness of each individual is computed. The fitness assignment strategy of SPEA2 considers for each solution, the number of solutions that dominate it and that are dominated by it. Furthermore, it uses the nearest neighbor density approach to maintain the diversity, while the archive truncation method is used for preserving the boundary solutions.

(iii) **MOCell**: it is an adaptation of a canonical GA to the multi-objective field [51]. The additional feature of MOCell is to return a number of solutions, from the archive to the population by randomly replacing existing individuals. This makes MOCell distinct from other multi-objective evolutionary algorithms. In MOCell, the individual is distributed according to a certain topology and only interacts with its nearby neighbors in the breeding loop. The most commonly-used population topology is 2-dimensional toroidal grids, which is adopted in this work.

(iv) **PREA:** it is proposed with the ratio based indicator. In PREA, a promising region is identified in the objective space using the ratio based indicator with infinite norm [52]. Since the individuals outside the promising region are the low-quality solutions, this method can discard these solutions from the current population. To ensure the diversity of population, a strategy based on the parallel distance is introduced to select individuals in the promising region. In this strategy, all individuals in the

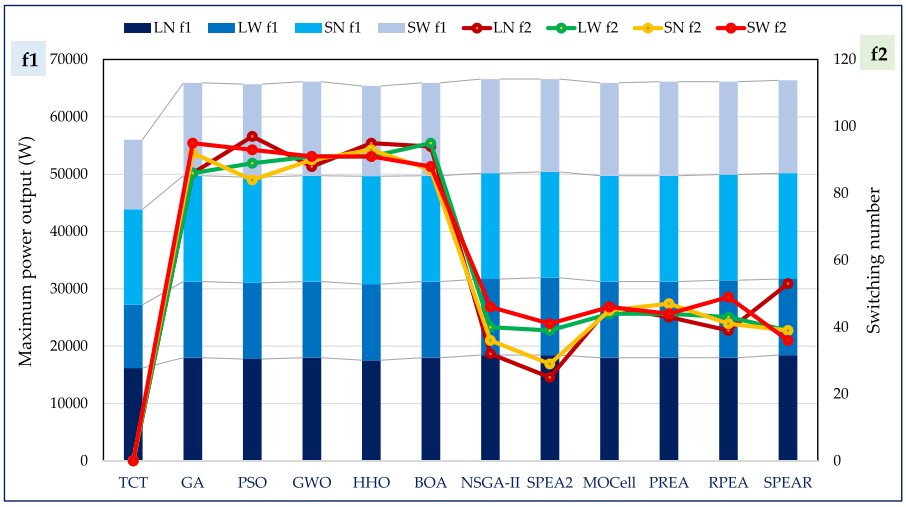

(a) 10×10 PV array

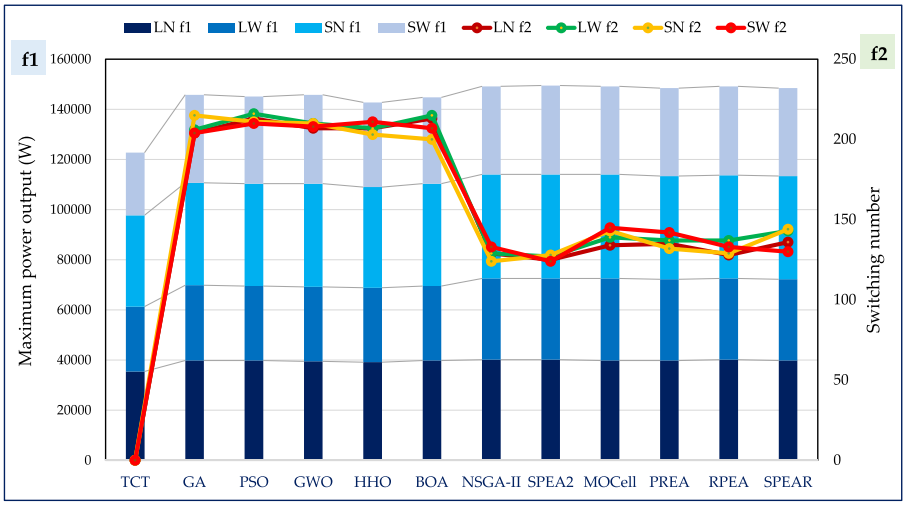

(b) 15×15 PV array

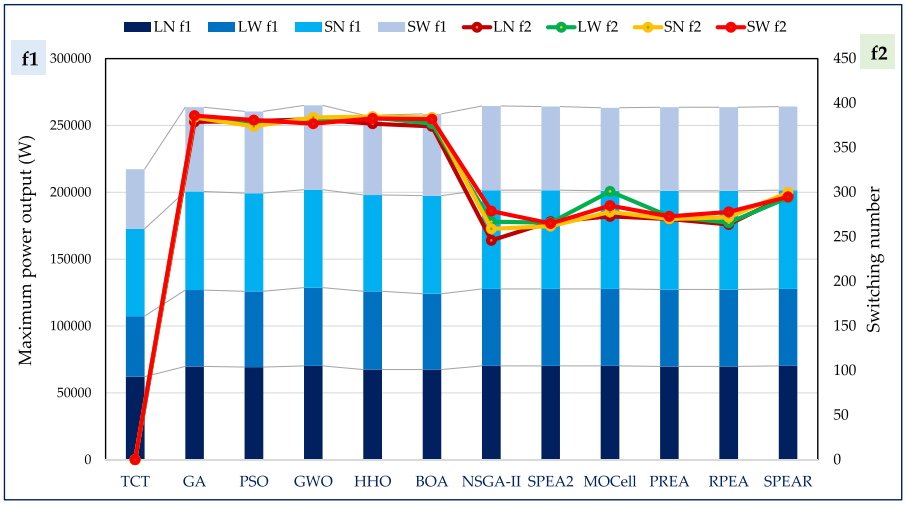

(c) 20×20 PV array

Fig. 21. The results comparison between different algorithms.

promising region are projected vertically onto the normal plane so that crowded distances between them can be calculated. Afterwards, two solutions with a smaller distance are selected from the candidate solutions each time, and the solution with the smaller indicator fitness value is removed from the current population.

(v) **RPEA:** it exploits the potential of the reference points-based approach to strengthen the selection pressure towards the Pareto front while maintaining an extensive and uniform distribution among solutions [53]. In RPEA, a series of reference points with good performances in convergence and distribution are continuously generated according to the current population to guide the evolution. Furthermore, the superior individuals are selected based on the evaluation of each individual by calculating the distances between the reference points and the individual in the objective space.

(vi) **SPEAR:** it is a substantial extension of early-developed prominent SPEA methods [54]. It inherits the advantage of fitness assignment of SPEA2 in quantifying solutions' diversity and convergence in a compact form, but replaces the most time-consuming density estimator by a reference direction based one. The fitness assignment also takes into account both local and global convergence.

3.2. Application design

From the viewpoint of optimization objectives and complexity, the most critical factors of the bi-objective PV array reconfiguration include the objective functions, the PV array scale, and the constraints of electrical switches. Note that the objective functions should be revealed in the fitness functions. The PV array scale directly influences the number of optimization variables, as well as for the optimization complexity. The constraints of electrical switches will directly influence the optimization performance, which should be carefully handled to match the continuous optimization variables.

3.2.1. Design of optimization variables

In the PV array reconfiguration, the optimization variables are discrete. However, the optimization variables in the presented evolutionary based Pareto optimization algorithms are regarded as the continuous variables by default. In this work, the optimization variables are set to be continuous in the searching operators of each algorithm, which will be only converted into the discrete variables in the calculation of fitness function. To satisfy the constraints in Eq. (9), the discrete variables are generated according to the ascending or descending orders of the continuous variables, as follows:

$$\boldsymbol{x}_{\mathrm{dis}} = \bigcup_{q=1}^{n_{\mathrm{col}}} sort\left(\boldsymbol{x}_{\mathrm{con}}^{q}\right)\# \tag{9}$$

where $\boldsymbol{x}_{\mathrm{dis}}$ denotes the matrix of discrete electricity switching states; $\boldsymbol{x}_{\mathrm{con}}^{q}$ denotes the vector of the continuous optimization variable for the PV strings at the qth column; and *sort* denotes the sorting order.

For example, the continuous optimization variables of a 5 × 5 PV array can be converted into the discrete variables according to the ascending order, as follows:

$$\boldsymbol{x}_{\mathrm{con}} = \begin{bmatrix} 2.3 & 4.4 & 4.1 & 3.9 & 1.3 \\ 0.7 & 1.2 & 3.3 & 0.8 & 2.9 \\ 1.5 & 3.8 & 0.2 & 0.6 & 3.7 \\ 5.2 & 2.1 & 0.5 & 5.7 & 5.1 \\ 2.4 & 0.9 & 4.9 & 4.0 & 2.5 \end{bmatrix} \Rightarrow \boldsymbol{x}_{\mathrm{dis}} = \begin{bmatrix} 3 & 5 & 4 & 3 & 1 \\ 1 & 2 & 3 & 2 & 3 \\ 2 & 4 & 1 & 1 & 4 \\ 5 & 3 & 2 & 5 & 5 \\ 4 & 1 & 5 & 4 & 2 \end{bmatrix} \# \tag{10}$$

3.2.2. Design of fitness functions

Since the constraints can be satisfied via the converting the variables, the fitness functions for each evolutionary based Pareto optimization algorithm can be directly designed according to the objective functions in Eq. (11). For the minimization of fitness functions, the original objective functions can be directly converted into the fitness functions, as.

$$\begin{cases} minF_1 \Leftrightarrow -maxf_1 = -V_{\mathrm{out}} \times I_{\mathrm{out}} \\ minF_2 \Leftrightarrow minf_2 = \sum_{p=1}^{n_{\mathrm{row}}} \sum_{q=1}^{n_{\mathrm{col}}} sign\left(\left| x_{pq}^{\mathrm{new}} - x_{pq}^{0} \right|\right) \end{cases} \# \tag{11}$$

where F_1 and F_2 are the fitness functions for the maximum power output and the minimum switching number, respectively.

3.2.3. Execution procedures

For the bi-objective PV array reconfiguration, the general execution procedure of evolutionary based Pareto optimization algorithm is given in Table 2, where $k_{\max}$ represents the maximum number of iterations. In general, the irradiation continuously changes over time. Along with this change, the bi-objective PV array reconfiguration should be re-executed for the non-uniform irradiation distribution (i.e., the partial shading condition). If there is no partial shadow, it does not implement any actions for the PV array. To avoid a frequent reconfiguration, the control time cycle of PV array reconfiguration can be set discretely (e.g., 5 min) in a practical application.

3.3. Best compromise reconfiguration scheme by TOPSIS

TOPSIS assumes that each attribute in the decision matrix takes either monotonically increasing or decreasing utility. In other words, a larger attribute outcome indicates more preference for the benefit criteria and less preference for the cost criteria. Furthermore, any outcome which is expressed in a nonnumerical way should be quantified through the appropriate scaling technique. Since all the criteria cannot be assumed to be of equal importance, the method receives a set of weights from the decision maker.

For the sake of simplicity, the operation of TOPSIS consists of the following steps:

Step 1: Construct the normalized decision matrix to transform the various attribute dimensions into nondimensional attributes, which allows comparison across the attributes. One way is to take the outcome of each criterion divided by the norm of the total outcome vector of the criterion at hand. An element r_{ij} of the normalized decision matrix $\boldsymbol{R}$ can be calculated as:

$$r_{ij} = \frac{y_{ij}}{\sqrt{\sum_{i=1}^{m} y_{ij}^{2}}}, i = 1, 2, \cdots, m\# \tag{12}$$

where y_{ij} is the numerical outcome of the ith alternative solution for the jth attribute.

Step 2: Construct the weighted norma1ized decision matrix via setting the weight vector given by the decision maker for each attribute to $\boldsymbol{w} = [\omega_1, \omega_2, \cdots, \omega_n]^T, \omega_1 + \omega_2 + \cdots + \omega_n = 1$, as.

$$v_{ij} = \omega_j \cdot r_{ij}, i = 1, 2, .., m, j = 1, 2, \cdots, n\# \tag{13}$$

Step 3: Determine the positive and negative ideal solutions, as follows:

$$A_j^{*} = \begin{cases} \max\limits_{i=1,2,\cdots,m} v_{ij}, \text{for a benefit attribute} \\ \min\limits_{i=1,2,\cdots,m} v_{ij}, \text{for a cost attribute} \end{cases} \# \tag{14}$$

$$A_j^- = \begin{cases} \min\limits_{i=1,2,\cdots,m} v_{ij}, \text{for a benefit attribute} \\ \max\limits_{i=1,2,\cdots,m} v_{ij}, \text{for a cost attribute} \end{cases} \# \quad (15)$$

where A_j^* denotes the jth attribute of the positive ideal solution and A_j^- denotes the jth attribute of the negative ideal solution.

Step 4: The separation between each alternative solution can be measured by the n-dimensional Euclidean distance, i.e., the distances from the ith alternative solution to the positive and negative ideal solutions, as.

$$s_i^* = \sqrt{\sum_{j=1}^{n} (v_{ij} - A_j^*)^2}, i = 1, 2, \cdots, m\# \quad (16)$$

$$s_i^- = \sqrt{\sum_{j=1}^{n} (v_{ij} - A_j^-)^2}, i = 1, 2, \cdots, m\# \quad (17)$$

Step 5: Calculate the relative closeness to the positive ideal solution, as.

$$c_i^* = \frac{s_i^-}{s_i^- + s_i^*}, 0 < c_i^* < 1, i = 1, 2, \cdots, m\# \quad (18)$$

Step 6: Rank the preference order according to the descending order of c_i^*, i.e., a larger relative closeness represents that the alternative solution is closer to the positive solution. Hence, the alternative solution with the largest relative closeness will be chosen as the best compromise solution, as.

$$\boldsymbol{x}_{\text{best}} = \underset{i=1,2,\cdots,m}{\text{argmax}} c_i^* \left(\boldsymbol{x}_i^{\text{PF}}\right) \# \quad (19)$$

where $\boldsymbol{x}_{\text{best}}$ denotes the best compromise solution and $\boldsymbol{x}_i^{\text{PF}}$ denotes the ith Pareto optimal solution.

4. Case studies

In order to test the performance of the proposed technique, three TCT connected PV arrays with different scales (i.e., 10 × 10, 15 × 15, 20 × 20) are introduced under four partial shadow patterns, including the long and narrow (LN) case, long and wide (LW) case, short and narrow (SN) case, short and wide (SW) case. For each PV array, the main parameters of PV module are given in Table 3. The standard temperature and irradiation are set to be 25 ℃ and 1000 W/m^2 in the following case studies. For each evolutionary based Pareto optimization algorithm, the maximum generations and population size are set to be 500 and 100, respectively. Except the maximum generations and population size, the other main parameters used in different evolutionary based Pareto optimization algorithms are given in Table 4.

For a practical implementation, the proposed PV array reconfiguration technique contains two processes. Firstly, it should find the optimal electrical switching scheme based on the real-time predictive data of irradiation and temperature, which is executed by a computer. Secondly, it should assign the action signals to all the switching devices, then the switching devices can response to the optimal electrical switching scheme. To verify the real-time response ability of each PV module, a real-time hardware-in-the-loop experiment has been carried out to evaluate the output feature under different weather conditions based on the RTLAB platform. Under different irradiations, the output curves of each PV module obtained by a hardware based RTLAB platform and a simulation based MATLAB are given in Fig. 3. It can be clearly seen that the output curves obtained by MATLAB are highly consistent with that obtained by RTLAB. Consequently, all the simulations are undertaken in MATLAB 9.11 with a multi-objective optimization toolbox called PlatEMO [55] by a personal computer with Intel(R) Core i7-10700 CPU at 2.9 GHz with 8 GB of RAM.

4.1. Pattern 1: Long and narrow case

In this case, long and narrow (LN) shading patterns for three different PV array are simulated. The shadow in this pattern is distributed broadly with four irradiance levels (i.e., 900, 700, 400, and 300 W/m^2) over several PV modules, where different colours mean different irradiance. The shade pattern 1 of the TCT-connected scheme for the 10 × 10 PV array is shown in Fig. 4. Apparently, the positions of PV modules in each column are uniformly distributed into different rows via PV array reconfiguration. Similarly, the irradiance distribution of LN for 15 × 15 PV array is shown in Fig. 6, in which the reconfiguration scheme is selected by TOPSIS from the multiple Pareto optimal solutions. For the PV reconfiguration scheme obtained by NSGA-II with TOPSIS in Fig. 4, the theoretical currents of all the rows currents can be calculated as follows:

$$\mathrm{I}_{\mathrm{R}_1} = 9\left(\frac{900}{1000}\right)\mathrm{I}_{\mathrm{M}} + \left(\frac{300}{1000}\right)\mathrm{I}_{\mathrm{M}} = 8.4\mathrm{I}_{\mathrm{M}}\# \quad (20)$$

$$\mathrm{I}_{\mathrm{R}_2} = 8\left(\frac{900}{1000}\right)\mathrm{I}_{\mathrm{M}} + \left(\frac{700}{1000}\right)\mathrm{I}_{\mathrm{M}} + \left(\frac{400}{1000}\right)\mathrm{I}_{\mathrm{M}} = 8.3\mathrm{I}_{\mathrm{M}}\#$$

$$\mathrm{I}_{\mathrm{R}_3} = 10\left(\frac{900}{1000}\right)\mathrm{I}_{\mathrm{M}} = 9\mathrm{I}_{\mathrm{M}}\# \quad (21)$$

$$\mathrm{I}_{\mathrm{R}_4} = 8\left(\frac{900}{1000}\right)\mathrm{I}_{\mathrm{M}} + \left(\frac{700}{1000}\right)\mathrm{I}_{\mathrm{M}} + \left(\frac{300}{1000}\right)\mathrm{I}_{\mathrm{M}} = 8.2\mathrm{I}_{\mathrm{M}}\# \quad (22)$$

$$\mathrm{I}_{\mathrm{R}_5} = \mathrm{I}_{\mathrm{R}_{10}} = 7\left(\frac{900}{1000}\right)\mathrm{I}_{\mathrm{M}} + \left(\frac{700}{1000}\right)\mathrm{I}_{\mathrm{M}} + 2\left(\frac{300}{1000}\right)\mathrm{I}_{\mathrm{M}} = 7.6\mathrm{I}_{\mathrm{M}}\# \quad (23)$$

$$\mathrm{I}_{\mathrm{R}_6} = \mathrm{I}_{\mathrm{R}_9} = 7\left(\frac{900}{1000}\right)\mathrm{I}_{\mathrm{M}} + \left(\frac{700}{1000}\right)\mathrm{I}_{\mathrm{M}} + 2\left(\frac{300}{1000}\right)\mathrm{I}_{\mathrm{M}} = 8.8\mathrm{I}_{\mathrm{M}}\# \quad (24)$$

$$\mathrm{I}_{\mathrm{R}_7} = \mathrm{I}_{\mathrm{R}_8} = 8\left(\frac{900}{1000}\right)\mathrm{I}_{\mathrm{M}} + 2\left(\frac{400}{1000}\right)\mathrm{I}_{\mathrm{M}} = 8\mathrm{I}_{\mathrm{M}}\# \quad (25)$$

where I_{M} is the current at the maximum power point per module and V_{M} is the voltage at the maximum power point per module.

Besides, the Pareto fronts derived by the different algorithms under LN case are given in Fig. 5. It can be found that each algorithm can only find a few Pareto optimal solutions for the PV array reconfiguration due to the low complexity under LN case. By integrating the Pareto optimal solutions obtained by all the evolutionary algorithms, a high-quality optimal Pareto front can be generated for the bi-objective PV array reconfiguration.

Similarly, the irradiance distribution of LN for 15 × 15 PV array is shown in Fig. 6. The evolutionary based Pareto optimization algorithms can effectively disperse the LN shadow. The Fig. 6 shows the reconfiguration scheme chosen by TOPSIS, which is to select one solution from Pareto front obtained by each evolutionary algorithm. According to the theoretical current outputs of all the rows, the theoretical maximum power outputs can be determined via a sorting comparison, as shown in Fig. 7. Firstly, it is clearly that the six evolutionary based Pareto optimization algorithms can acquire higher maximum power outputs against to TCT. Particularly, the maximum power outputs obtained by SPEA2, MOCell, and RPEA are 11.1 % larger than that of TCT without optimization on the 10 × 10 PV array. On the other hand, it is comprehensible from Fig. 8 that the all the six evolutionary based Pareto optimization algorithms can significantly reduce the row current difference compared to the TCT scheme without optimization. This is the main reason why the mismatch loss can be reduced and the maximum power output can be dramatically increased.

4.2. Pattern 2: Long and wide case

For the LW shade pattern, the shadow covers with five different irradiations (i.e., 900, 600, 500, 400 and 200 W/m^2). It is clear that each

algorithm will provide multiple feasible solutions for PV reconfiguration. Among in the multiple Pareto optimal solutions, the only one compromise solution is chosen by TOPSIS as shown in Fig. 9. In Fig. 9, different reconfiguration schemes of the 10 × 10 and 15 × 15 PV arrays obtained by the evolutionary based Pareto optimization algorithms indicate that the shadows can be evenly dispersed throughout the array, which can effectively reduce the damage to PV panels.

The theoretical maximum power outputs of the 10 × 10 and 15 × 15 PV arrays are given in Fig. 10. In the 10 × 10 PV array, the performance difference between different evolutionary based Pareto based optimization algorithms is slight, in which NSGA-II, MOCell, RPEA, and SPEAR have the same theoretical maximum output power. As the scale of PV array increases, the performance difference between different evolutionary based Pareto based optimization algorithms increases obviously. Fig. 11 shows the boxplot of row currents on a 10 × 10 and 15 × 15 PV array under LW case. It is clear that the row current difference by TCT is much larger than that by each evolutionary based Pareto based optimization algorithm.

Fig. 12 provides the Pareto fronts obtained by the six evolutionary based Pareto optimization algorithms. It illustrates that each algorithm can only find several Pareto optimal solutions for the PV array reconfiguration under LW case, but they can be integrated into an approximate ideal Pareto surface for different scales of PV arrays. As shown in Fig. 12, each Pareto optimization algorithm can provide at least two optimal solutions to rearrange the PV array. Based on the TOPSIS, the compromised solution is chosen and the corresponding irradiation distributions is shown in Fig. 9.

4.3. Pattern 3: Short and narrow case

In the SN shade pattern, each PV array only experiences three irradiation variations (i.e., 900, 600 and 400 W/m^2), as depicted in the Fig. 13. In Fig. 13, the chosen compromise solution of 10 × 10 and 15 × 15 PV reconfiguration is presented. Through column reconstruction, the shadows of 10 × 10 and 15 × 15 PV array are effectively dispersed based on the compromise solution.

Due to the low complexity of SN shade pattern, the performance of each evolutionary based Pareto optimization algorithm is quite close, as shown in Fig. 14. Moreover, the largest increment of maximum power output between NSGA-II and TCT is 13.9 %. Similarly, all the six different evolutionary algorithms can obtain the much smaller row current differences than that of TCT, as shown in Fig. 15.

Fig. 16 provides the Pareto fronts derived by six different algorithms under the SN shade pattern. Fig. 16 shows the solutions obtained by SPEAR deviate distinctly from the idea Pareto front, in which the performance of NSGA-II, RPEA, and PREA are superior to SPEAR. Meanwhile, the Pareto optimal solutions of NSGA-II and PREA are distributed more evenly and widely than that of other algorithms.

4.4. Pattern 4: Short and wide case

As shown in Fig. 17, the SW shade pattern consists of four different irradiations (i.e., 900, 600, 400 and 200 W/m^2) over the 10 × 10 and 15 × 15 PV array. Besides, the Pareto fronts derived by the six different evolutionary based Pareto optimization algorithms are given in Fig. 20. The quality of the Pareto front obtained by SPEA2 is the highest among all the algorithms, while the number of Pareto optimal solutions obtained by SPEAR is the largest. Furthermore, the number of Pareto optimal solutions in the SW shade pattern is more than that in other three patterns. As a result, the diversity of Pareto solutions can be guaranteed.

Based on the reconfiguration schemes acquired by the different evolutionary Pareto-based optimization algorithms chosen by TOPSIS in Fig. 17, the maximum power output can be dramatically increased by each evolutionary based Pareto optimization algorithm, as shown in Fig. 18. For the 15 × 15 PV array, the maximum power outputs of NSGA-II, SPEA2, MOCell, PREA, RPEA, and SPEAR are increased by 35.1 %, 37.8 %, 33.7 %, 35.1 %, 33.7 %, and 27 % compared to the TCT without optimization, respectively. Besides, the difference of rwo current distributions between evolutionary based Pareto optimization algorithms and TCT is much larger than that of other cases, as given in Fig. 19.

4.5. Statistical studies

Here, six existing PV array reconfiguration techniques including TCT without optimization [6], GA [33], PSO [35], GWO [38], HHO [34], and BOA [37], are introduced to compare with the evolutionary based Pareto optimization algorithms. The last five algorithms are single-objective *meta*-heuristic optimization algorithms for the maximization of power output. Fig. 21 shows the results comparison between different algorithms on different PV arrays under four patterns. Two conclusions can be summarized from Fig. 21, as follows:

- Firstly, the maximum power outputs (f_1) of the best solutions by all the evolutionary based Pareto optimization algorithms are larger than that by each single-objective *meta*-heuristic algorithm in most cases. The increment of maximum power output is up to 10.23 % between MOCell and PSO on the 15 × 15 PV array under the LW shade pattern. Compared with GWO and HHO, the maximum power output increases 2.5 % and 5.1 % for the 10 × 10 PV array under LN shade. Under the SW shade pattern, the maximum power output obtained by PREA is 41.89 % larger than that of TCT without optimization for the 15 × 15 PV array. Besides, the difference on the maximum power output between the compromise solution by all the evolutionary based Pareto optimization algorithms and single-objective algorithms is slight.
- Secondly, the switching number (f_2) of electrical connections by all the evolutionary based Pareto optimization algorithms can be dramatically reduced compared with each single-objective *meta*-heuristic algorithm. For the best solution, the switching number obtained by PSO is up to 3.88 times of that by SPEA2 on the 10 × 10 PV array under the LW shade pattern. Compared with single-objective *meta*-heuristic optimization algorithms, all the evolutionary based Pareto optimization algorithms for bi-objective PV array reconfiguration can reduce the switching times by at least half under different cases.

5. Conclusion

In summary, the proposed evolutionary based Pareto optimization algorithms for the bi-objective PV array reconfiguration have the following contributions:

(1) The conventional PV array reconfiguration mainly focuses on the generation efficiency improvement under PSC. In contrast, the constructed bi-objective PV array reconfiguration can further reduce the switching control complexity except improving the generation efficiency.
(2) Various powerful evolutionary based Pareto optimization algorithms are designed for the bi-objective PV array reconfiguration, which can provide multiple alternative Pareto optimal reconfiguration schemes to the PV array. Compare with the single-objective optimization with only one optimal scheme, the PV array can select a best compromise PV array reconfiguration scheme from the multiple Pareto optimal solutions. This is beneficial to improve the flexibility of PV array reconfiguration under various irradiation conditions.
(3) Simulation results under four different patterns demonstrate that the compromise solutions of the evolutionary Pareto-based optimization algorithms can obtain the same or better maximum power output than TCT without optimization and the single-

objective optimization algorithms, while the number of switches is significantly decreased.

CRediT authorship contribution statement

Xiaoshun Zhang: Conceptualization, Writing – review & editing. **Die Meng:** Methodology, Writing – original draft. **Wenji Li:** Software, Supervision. **Tao Yu:** Investigation, Validation. **Zhun Fan:** Funding acquisition. **Zhifeng Hao:** Project administration.

Declaration of Competing Interest

The authors declare that they have no known competing financial interests or personal relationships that could have appeared to influence the work reported in this paper.

Data availability

Data will be made available on request.

Acknowledgements

This work was jointly supported by National Natural Science Foundation of China (51907112, U2066212), Natural Science Foundation of Guangdong Province of China (2019A1515011671), STU Scientific Research Foundation for Talents (NTF21001), Science and Technology Planning Project of Guangdong Province of China (2019A050520001, 2021A0505030072), Science and Technology Special Funds Project of Guangdong Province of China (STKJ2021176), and Fundamental Research Funds for the Central Universities (N2229001).

References

[1] Taheri A, Kazemi M, Amini M, Sardarabadi M, Kianifar A. The performance assessment of nanofluid-based PVTs with and without transparent glass cover: outdoor experimental study with thermodynamics analysis. J Therm Anal Calorim 2021;143(6):4025–37.
[2] Lappalainen K, Kleissl J. Analysis of the cloud enhancement phenomenon and its effects on photovoltaic generators based on cloud speed sensor measurements. J Renewable Sustainable Energy 2020;12(4). Art. no. 043502.
[3] Ajmal AM, Ramachandaramurthy VK, Naderipour A, Ekanayake JB. Comparative analysis of two-step ga-based PV array reconfiguration technique and other reconfiguration techniques. Energy Convers Manage 2021;230. Art. no. 113806.
[4] Malathy S, Ramaprabha R. Reconfiguration strategies to extract maximum power from photovoltaic array under partially shaded conditions. Renew Sustain Energy Rev 2018;81:2922–34.
[5] Dhanalakshmi B, Rajasekar N. A novel competence square based PV array reconfiguration technique for solar PV maximum power extraction. Energy Convers Manage 2018;174:897–912.
[6] Sagar G, Pathak D, Gaur P, Jain V. A sudoku puzzle based shade dispersion for maximum power enhancement of partially shaded hybrid bridge-link-total-cross-tied PV array. Sol Energy 2020;204:161–80.
[7] Wang YJ, Hsu PC. An investigation on partial shading of PV modules with different connection configurations of PV cells. Energy 2011;36(5):3069–78.
[8] Bastidas-Rodr´ıguez JD, Trejos-Grisales LA, Gonzalez-Montoya D, Ramos-Paja CA, Petrone G, Spagnuolo G. General modeling procedure for photovoltaic arrays. Electric Power Systems Research 2018;155:67–79.
[9] Saiprakash C, Mohapatra A, Nayak B, Ghatak SR. Analysis of partial shading effect on energy output of different solar PV array configurations. Mater Today: Proc 2021;39:1905–9.
[10] Belhachat F, Larbes C. Modeling, analysis and comparison of solar photovoltaic array configurations under partial shading conditions. Sol Energy 2015;120:399–418.
[11] Kaushika ND, Gautam NK. Energy yield simulations of interconnected solar PV arrays. IEEE Trans Energy Convers 2003;18(1):127–34.
[12] Bingol O, Ozkaya B. Analysis and comparison of different PV array configurations under partial shading conditions. Solar Energy 2018;160:336–43.
[13] Yang B, Zhu T, Wang J, Shu H, Yu T, Zhang X, et al. Comprehensive overview of maximum power point tracking algorithms of PV systems under partial shading condition. J Cleaner Prod 2020;268. Art. no. 121983.
[14] Ajmal AM, Thanikanti SB, Ramachandaramurthy VK, Ekanayake J, and Tariq M. "Effect of partial shading and performance analysis on various array configurations of photovoltaic system". In: 2019 9th International Conference on Power and Energy Systems (ICPES), Perth, Australia, pp. 1–6, 2019.
[15] Nguyen D, Lehman B. An adaptive solar photovoltaic array using model-based reconfiguration algorithm. IEEE Trans Ind Electron 2008;55(7):2644–54.
[16] Potnuru SR, Pattabiraman D, Ganesan SI, Chilakapati N. Positioning of PV panels for reduction in line losses and mismatch losses in PV array. Renewable Energy 2015;78:264–75.
[17] Horoufiany M, Ghandehari R. Optimization of the sudoku based reconfiguration technique for PV arrays power enhancement under mutual shading conditions. Sol Energy 2018;159:1037–46.
[18] Krishna SG, Moger T. Optimal sudoku reconfiguration technique for total-cross-tied PV array to increase power output under nonuniform irradiance. IEEE Trans Energy Convers 2019;34(4):1973–84.
[19] Krishna GS, Moger T. Improved sudoku reconfiguration technique for total-cross-tied PV array to enhance maximum power under partial shading conditions. Renew Sustain Energy Rev 2019;109:333–48.
[20] Ye C-E, Tai C-C, Huang Y-P, Chen J-J. Dispersed partial shading effect and reduced power loss in a PV array using a complementary sudoku puzzle topology. Energy Convers Manage 2021;246. Art. no.114675.
[21] Pillai DS, Rajasekar N, Ram JP, Chinnaiyan VK. Design and testing of two-phase array reconfiguration procedure for maximizing power in solar PV systems under partial shade conditions (psc). Energy Convers Manage 2018;178:92–110.
[22] Dhanalakshmi B, Rajasekar N. Dominance square based array reconfiguration scheme for power loss reduction in solar photovoltaic (PV) systems. Energy Convers Manage 2018;156:84–102.
[23] Venkateswari R, Rajasekar N. Power enhancement of PV system via physical array reconfiguration based lo shu technique. Energy Convers Manage 2020;215. Art. no. 112885.
[24] Kumar BP, Cherukuri SK, Kaniganti KR, Karuppiah N, Muniraj R, Babu TS, et al. Performance enhancement of partial shaded photovoltaic system with the novel screw pattern array configuration scheme. IEEE Access 2021;10:1731–44.
[25] Cherukuri SK, Kumar BP, Kaniganti KR, Muthubalaji S, Devadasu G, Babu TS, et al. A novel array configuration technique for improving the power output of the partial shaded photovoltaic system. IEEE Access 2022;10:15056–67.
[26] Velasco-Quesada G, Guinjoan-Gispert F, Piqu´e-L´opez R, Roní an-Lumbreras M, and ConesaRoca A. "Electrical PV array reconfiguration strategy for energy extraction improvement in grid-connected PV systems". IEEE Transactions on Industrial Electronics, 2009; 56(11): 4319–4331.
[27] Huang Y-P, Chen X, Ye C-E. Implementation of a modified circuit reconfiguration strategy in high concentration photovoltaic modules under partial shading conditions. Sol Energy 2019;194:628–48.
[28] Srinivasan A, Devakirubakaran S, Sundaram BM. Mitigation of mismatch losses in solar PV system two-step reconfiguration approach. Sol Energy 2020;206:640–54.
[29] Satpathy PR, Sharma R. Power and mismatch losses mitigation by a fixed electrical reconfiguration technique for partially shaded photovoltaic arrays. Energy Convers Manage 2019;192:52–70.
[30] Rajan NA, Shrikant KD, Dhanalakshmi B, Rajasekar N. Solar PV array reconfiguration using the concept of standard deviation and genetic algorithm. Energy Procedia 2017;117:1062–9.
[31] Karakose M, Baygin M, and Parlak KS. "A new real-time reconfiguration approach based on neural network in partial shading for PV arrays". In: 2014 International Conference on Renewable Energy Research and Application (ICRERA), Milwaukee, USA, pp. 633–637, 2014.
[32] Mahmoud A, Shamseldein M, Hasanien H, and Abdelaziz A. "Photovoltaic array reconfiguration to reduce partial shading losses using water cycle algorithm". In: 2019 IEEE Electrical Power and Energy Conference (EPEC), Montreal, Canada, pp. 1–6, 2019.
[33] Deshkar SN, Dhale SB, Mukherjee JS, Babu TS, Rajasekar N. Solar PV array reconfiguration under partial shading conditions for maximum power extraction using genetic algorithm. Renew Sustain Energy Rev 2015;43:102–10.
[34] Yousri D, Allam D, Eteiba MB. Optimal photovoltaic array reconfiguration for alleviating the partial shading influence based on a modified harris hawks optimizer. Energy Convers Manage 2020;206. Art. no. 112470.
[35] Bayoumi ASA, El-Sehiemy RA, Abaza A. Effective PV parameter estimation algorithm based on marine predators optimizer considering normal and low radiation operating conditions. Arabian Journal for Science and Engineering 2022;47(3):3089–104.
[36] Yousri D, Thanikanti SB, Balasubramanian K, Osama A, Fathy A. Multi-objective grey wolf optimizer for optimal design of switching matrix for shaded PV array dynamic reconfiguration. IEEE Access 2020;8:159931–46.
[37] Fathy A. Butterfly optimization algorithm based methodology for enhancing the shaded photovoltaic array extracted power via reconfiguration process. Energy Convers Manage 2020;220. Art. no. 113115.
[38] Mohanty S, Subudhi B, Ray PK. A new mppt design using grey wolf optimization technique for photovoltaic system under partial shading conditions. IEEE Trans Sustainable Energy 2015;7(1):1–8.
[39] Yousri D, Babu TS, Mirjalili S, Rajasekar N, Abd Elaziz M. A novel objective function with artificial ecosystem-based optimization for relieving the mismatching power loss of large-scale photovoltaic array. Energy Convers Manage 2020;225. Art. no. 113385.
[40] Yang B, Shao R, Zhang M, Ye H, Liu B, Bao T, et al. Socio-inspired democratic political algorithm for optimal PV array reconfiguration to mitigate partial shading. Sustainable Energy Technol Assess 2021;48. Art. no. 101627.
[41] Zhang X, Li C, Li Z, Yin X, Yang B, Gan L, et al. Optimal mileage-based PV array reconfiguration using swarm reinforcement learning. Energy Convers Manage 2021;232. Art. no. 113892.
[42] Zhang X, Yu T, Ma X, Guo L. An efficient multi-agent negotiation algorithm for multi-period photovoltaic array reconfiguration with a hydrogen energy storage system. Energy Convers Manage 2022;256. Art. no. 115376.

[43] Mostafaee G, Ghandehari R. Power enhancement of photovoltaic arrays under partial shading conditions by a new dynamic reconfiguration method. Journal of Energy Management and Technology 2020;4(1):46–51.
[44] Ajmal AM, Babu TS, Ramachandaramurthy VK, Yousri D, Ekanayake JB. Static and dynamic reconfiguration approaches for mitigation of partial shading influence in photovoltaic arrays. Sustainable Energy Technol Assess 2020;40. Art. no. 100738.
[45] Almaktar M, Rahman HA, and Hassan MY. "Effect of losses resistances, module temperature variation, and partial shading on PV output power". In: 2012 IEEE International Conference on Power and Energy (PECon), Kota Kinabalu, Malaysia, pp. 360–365, 2012.
[46] Vankadara SK, Chatterjee S, Balachandran PK. An accurate analytical modeling of solar photovoltaic system considering Rs and Rsh under partial shaded condition. International Journal of System Assurance Engineering and Management 2022. https://doi.org/10.1007/s13198-022-01658-6.
[47] Humada AM, Hojabri M, Mekhilef S, Hamada HM. Solar cell parameters extraction based on single and double-diode models: A review. Renew Sustain Energy Rev 2016;56:494–509.
[48] Paví c Z. and Novoselac V. "Notes on TOPSIS method," International Journal of Research in Engineering and Science, 2013; 1(2):5–12.
[49] Deb K, Pratap A, Agarwal S, Meyarivan T. A fast and elitist multi-objective genetic algorithm: NSGA-II. IEEE Trans Evol Comput 2002;6(2):182–97.
[50] Zitzler E, Laumanns M, Thiele L. Spea2: Improving the strength pareto evolutionary algorithm. TIK-report 2001;103.
[51] Nebro AJ, Durillo JJ, Luna F, Dorronsoro B, Alba E. Mocell: A cellular genetic algorithm for multi-objective optimization. Int J Intell Syst 2009;24(7):726–46.
[52] Yuan J, Liu H-L, Gu F, Zhang Q, He Z. Investigating the properties of indicators and an evolutionary many-objective algorithm using promising regions. IEEE Trans Evol Comput 2020;25(1):75–86.
[53] Liu Y, Gong D, Sun X, Zhang Y. Many-objective evolutionary optimization based on reference points. Appl Soft Comput 2017;50:344–55.
[54] Jiang S, Yang S. A strength pareto evolutionary algorithm based on reference direction for multiobjective and many-objective optimization. IEEE Trans Evol Comput 2017;21(3):329–46.
[55] Tian Y, Cheng R, Zhang X, Jin Y. PlatEMO: A MATLAB platform for evolutionary multi-objective optimization educational forum. IEEE Comput Intell Mag 2017;12 (4):73–87.